

## Review

## A review of laser welding for aluminium and copper dissimilar metals

Bo Ma<sup>a</sup>, Xiangdong Gao<sup>a,\*</sup>, Yijie Huang<sup>a</sup>, Perry P. Gao<sup>b</sup>, Yanxi Zhang<sup>a</sup><sup>a</sup> Guangdong Provincial Welding Engineering Technology Research Center, Guangdong University of Technology, Guangzhou, China<sup>b</sup> Education Bridge Institute, Boston, USA

## ARTICLE INFO

**Keywords:**  
 Al/Cu dissimilar metals  
 Laser welding  
 Welding process  
 Filler metals  
 Process monitoring

## ABSTRACT

Dissimilar metal composite structures have been used in a wide range of applications to meet the requirements of lightness, corrosion resistance, electrical conductivity, and thermal conductivity due to their excellent overall performance. With the global energy conservation and emission reduction policies, dissimilar aluminium (Al) and copper (Cu) for lithium battery welding are more and more discussed. Laser welding is a unique technology for Al and Cu due to its high energy density, precise control, ease of automation, and remote welding. However, high reflectivity and differences in material properties result in poor laser absorption and an unstable welding process. Furthermore, sufficient mixing of Al and Cu during the welding process tends to form brittle intermetallic compounds (IMCs). This paper discusses the laser welding and the challenges faced by joining Al/Cu dissimilar metals, and analyzes the effect of different process parameters and laser output modes on the weld joint. Furthermore, the research progress on filler metals and process monitoring are discussed.

## 1. Introduction

As manufacturing upgrades are accelerated, the performance of various weld structures is becoming increasingly demanding. It must satisfy traditional mechanical properties and electrical conductivity, thermal conductivity, and corrosion resistance requirements. It is difficult for a single metal to meet all these different requirements. Al and Cu can not only take full advantage of the excellent properties of various substrates but are also lightweight and reduce production costs. They are widely used in aerospace, shipbuilding, automotive manufacturing, electronics, and heat exchanger [1–3]. The new energy automobile industry is booming with the development of global energy conservation and emissions reduction policies. As a result, manufacturers have been forced to seek more efficient power systems and lighter materials to reduce energy consumption [4–6]. An essential component of electric vehicle power supplies is the application of large numbers of lithium-ion batteries in series or parallel [7–9]. Scholars have widely discussed welding technology of Al and Cu for lithium-ion battery electrode ears. The Al-Cu joint is expected to have good mechanical properties, electrical and thermal conductivity, corrosion resistance, and excellent fatigue life. Since the difference in physical and chemical performances [10,11], it is difficult for Cu to dissolve into Al during welding, and results in defects such as cracks, porosity, and brittle IMCs in the welded joint. The brittle IMCs reduce the mechanical strength and the corrosion

resistance of the joints, and increase the contact resistance [12–14].

The welding process for Al/Cu dissimilar metals has been divided into solid-state and fusion welding. In solid-state welding, the surface of the metal is softened below the melting point, allowing Al and Cu to disperse towards one another under external pressure and form a joint [15], including friction stir welding [10,16–19], ultrasonic welding [20,21], magnetic pulse welding [22–24]. In fusion welding, heat sources are generated that cause the metals to melt and undergo metallurgical reactions, and form a joint upon cooling and solidification [25], including resistance spot welding [26–28], electron beam welding [29–31], laser beam welding [32–34], as well as laser brazing [35–40]. Table 1 compares different welding technologies for Al/Cu. Solid-state welding is often used in multi-layer lap welding of Al/Cu dissimilar metals due to the low heat generated and the reduction of IMCs' formation. However, solid-state welding destroyed the integrity of the grain structure, leading to the unevenness of the substrate. The fusion welding process is inevitably exposed to thermal cracking, porosity, and IMC defects. By controlling and optimizing the parameters of the fusion welding process with high accuracy, the defects can be reduced to some degree, and good joints can be obtained to meet the production requirements.

Laser beam welding, as a fusion welding technique, allows the materials to absorb the energy of laser radiation, convert it into heat, melt the metal, and form a molten pool. When the temperature of the molten

\* Corresponding author.

E-mail address: [gaoxd@gdut.edu.cn](mailto:gaoxd@gdut.edu.cn) (X. Gao).

**Table 1**

Applications, advantages, and disadvantages of different welding techniques for Al and Cu.

Welding technology	Applications	Advantages	Disadvantages
Friction stir welding	<ul style="list-style-type: none"> <li>Butt welding of Al/Cu</li> <li>Heat exchanger</li> </ul>	<ul style="list-style-type: none"> <li>Low thermal crack and porosity</li> <li>Reduce the formation of IMCs</li> </ul>	<ul style="list-style-type: none"> <li>Design limitation for tooling by material and joint type</li> <li>Tooling wear</li> <li>Cold cracks and holes</li> </ul>
Ultrasonic welding	<ul style="list-style-type: none"> <li>Multi-layer lap welding of Al/Cu</li> <li>Connection of battery cells and busbars in the Model-S</li> </ul>	<ul style="list-style-type: none"> <li>Short welding time and energy input</li> </ul>	<ul style="list-style-type: none"> <li>Destruction of the metal structure by ultrasonic vibration</li> <li>Sensitive to surface roughness</li> <li>Raising welding temperature by high-frequency vibration</li> <li>Soft metal surface by high pressure</li> </ul>
Magnetic pulse welding	<ul style="list-style-type: none"> <li>Al/Cu welding of lithium-ion batteries and connector terminals</li> </ul>	<ul style="list-style-type: none"> <li>Low heat and IMCs</li> <li>Short welding time</li> </ul>	
Resistance spot welding	<ul style="list-style-type: none"> <li>Spot welding of Al/Cu</li> </ul>	<ul style="list-style-type: none"> <li>Low cost</li> <li>Easy automation</li> <li>Efficient</li> </ul>	<ul style="list-style-type: none"> <li>Limited by material thickness</li> <li>Requiring high current for welding Al/Cu</li> <li>Hot cracking</li> <li>IMCs formation</li> </ul>
Electron beam welding	<ul style="list-style-type: none"> <li>Welding Al/Cu on the space station</li> </ul>	<ul style="list-style-type: none"> <li>High energy density</li> <li>High energy conversion</li> <li>High precision</li> <li>Large depth-to-width ratio</li> <li>Small heat-affected zone</li> </ul>	<ul style="list-style-type: none"> <li>Complicated and expensive equipment</li> <li>Vacuum the working environment</li> <li>Easily disturbed by the magnetic field</li> <li>Hot cracking</li> <li>IMCs formation</li> </ul>
Laser welding and laser brazing	<ul style="list-style-type: none"> <li>Lithium-ion battery electrode ears</li> <li>Current collectors</li> </ul>	<ul style="list-style-type: none"> <li>High energy density</li> <li>High precision</li> <li>Small heat-affected zone</li> <li>Large depth-to-width ratio</li> <li>High-speed welding</li> <li>Remoting welding</li> </ul>	<ul style="list-style-type: none"> <li>Hot cracking and porosity</li> <li>IMCs formation</li> <li>Low laser absorption of Al and Cu</li> <li>High power requirements</li> <li>Expensive equipment</li> </ul>

pool increases with the power density ( $5 \times (10^6\text{--}10^7)$  W·cm $^{-2}$ ) of the material above the boiling point, the molten pool begins to evaporate, forming a cavity or hole, then the metal atoms diffuse, fuse, and rapidly cool and solidify to form a welded joint [41–43]. Laser welding has the characteristics of a high energy density and a small heat-affected zone; it is easy to achieve high speed and high-precision control, and adapt to various work environments. The laser beam can be transmitted over long distances through optical fiber, realizing remote welding with a corresponding telephoto lens and a high-quality beam [44–46]. However, high-energy density welding joint is susceptible to cracks and pores [47–50]. When laser welding metals, the absorption efficiency of metal to laser radiation is inversely proportional to its conductivity. Therefore, high reflectively materials such as Al, Cu, and magnesium (Mg) have weak ability to absorb laser radiation [51–54]. This has also become a challenge for laser welding such metals. With the improvement of the welding process and the cost reduction, laser welding has become the most anticipated technology for dissimilar metal welding because of its high efficiency, contact-free, and automation. Compared

with other welding technologies, the advantages of laser welding Al and Cu are as follows:

- Laser welding can achieve high speed, high precision, and large-scale automated manufacturing with high stability and repeatability to meet various occasions and technical requirements.
- The high energy density and small heat-affected zone allow laser welding to achieve deep penetration welding and obtain welded joints with a high depth-to-width ratio.
- Laser welding can realize non-contact remote welding and facilitate the installation of various sensors for online monitoring and closed-loop control.

However, laser welding Al and Cu has some limitations:

- Hot cracking and porosity occur easily during the laser welding process.
- Low energy conversion efficiency of near-infrared laser for welding non-ferrous metals.
- Al and Cu atoms diffuse strongly during laser welding, and more IMCs are easily produced in welded joints.

Laser welding of dissimilar metals is highly valued and has become a separate branch of laser material processing. At present, several review papers on laser welding of Al/Cu dissimilar metals focus on applications in battery manufacturing. However, they mainly study the effect of laser parameters or filler metals on the quality of welded joints [5,8,56–58] and a detailed and in-depth discussion of the function mechanism of process parameters, control strategies for IMCs, and process monitoring in the application of Al/Cu laser welding are not provided. Providing generic knowledge beyond the laser welding parameters is of great significance. Such as the fundamental underlying physics of different parameters, the effect of remelting and solidification in the fusion zone caused by different laser output methods, and the role they play via laser absorption, temperature fields, driving forces, fluid flow, metal mixing, microstructure formation, and eventually mechanical or electrical properties.

This paper reviews some aspects of Al/Cu dissimilar metal laser welding technology: describes the faced challenges and the impact of IMCs on the mechanical and electrical properties of the joint; analyzes the mechanisms of different process parameters on laser absorption, molten pool flow, and metal mixing; discusses temperature gradient and solidification rate of the molten pool under different laser output modes and the positive effect on the suppression of defects to improve the quality of the weld; summarizes the influence of the filler metal on the quality of the joint; introduces the principles of monitoring systems and the relation between the observed object and defect formation or weld quality. The aim is to provide a reasonable basis for producing reliable laser welding of Al and Cu dissimilar metals and proposes possible subjects for future research.

**Table 2**

The physical properties of Al and Cu [55].

Metals	Al	Cu
Melting point (K)	933	1356
Boiling point (K)	2793	2833
Density (kg·m $^{-3}$ )	2700	8930
Thermal conductivity coefficient (W·m $^{-1}\cdot\text{K}^{-1}$ )	238	397
Specific heat capacity (J·Kg $^{-1}\cdot\text{K}^{-1}$ )	917	386
Thermal expansion coefficient ( $\times 10^6\cdot\text{K}^{-1}$ )	23.5	17

## 2. Challenges of Al/Cu laser welding

### 2.1. Different material properties

The physical properties of Al and Cu metals are shown in Table 2 [55]. Differences in melting point and specific heat capacity can cause Al to melt before Cu has yet to reach its melting point, and the Cu will only soften or melt in a small area of the surface. Differences in the thermal conductivity coefficient and thermal expansion lead to the stress concentrations at the joint interface with the formation of holes and cracks [14]. The schematic diagram of different types of porosity formation mechanisms in the Al-Cu laser welding process is shown in Fig. 1. A keyhole appears at the bottom of the molten pool due to the recoil pressure of the metal vapor. However, the flow of molten Al is poor, and the keyhole can collapse due to the rapid cooling rate. When the back-filling rate of molten metal is much lower than the solidification rate, internal porosity is created. It remains at the bottom of the molten pool as it solidifies (Porosity I). Some porosity flow along the molten pool to the Al side (Porosity II) or escapes along the keyhole (Porosity III). In addition, the cavitation of contaminants on the surface of Al with H, O, or N elements can also cause the appearance of porosity (Porosity II) [59]. The excellent thermal conductivity of Cu also exacerbates the cooling of Al, increasing the susceptibility of Al to porosity during welding [7].

The difference in thermal expansion coefficients and solidification rates produce hole cracks at the joint interface. In addition, their poor mutual solubility also leads to IMCs that can cause grain boundary cracking. The schematic diagram of the crack formation in Al-Cu joints is shown in Fig. 2. During the laser welding process of Al and Cu, Cu atoms penetrate along the grain boundaries of Al. Al and Cu react at high temperatures to form Al-Cu eutectic, which facilitates the improvement of the mechanical properties of the joint. Due to the rapid cooling rate, some Cu atoms react with Al to form Al-Cu IMCs. The thermal stresses at this stage are small, and the plastic deformation of the grains balances the thermal stresses generated at the grain boundaries. Therefore, no liquefied cracking is formed. In the following stage, cracks start to sprout, IMCs are enriched at the grain boundaries, and the cohesion between grains is reduced, resulting in thermal stresses in the weld that cannot be completely neutralized. Due to the thermal cycling, the intergranular bonding is further weakened with the increasing liquefaction zone. The thermal stress increases significantly with heat input, and cracks expand. At the same time, microcracks can become new crack sources and proliferate along the grain boundaries, thus forming large cracks in series.

### 2.2. Low laser absorption efficiency

Since the transmittance of metal is 0, only absorption and reflection occur when the laser beam is irradiated on the metal. Laser absorption efficiency in metals is almost proportional to the electrical conductivity, as the valence electrons in metals move freely in crystals, making it difficult for lasers to be absorbed in low energies [60]. However, when the laser energy density is high enough, the energy absorbed by the intraband transition of free electrons is converted into heat energy, causing the rise of the temperature of the metal. As shown in Fig. 3, the laser absorption efficiency of metals depends on the laser wavelength [61]. The higher the wavelength of the laser, the lower the absorption efficiency by irradiated materials. In the case of Al and Cu, for example, when the laser wavelength is about 1 μm, the absorption efficiency of the laser is less than 20% for Al and less so the Cu, only about 10%. Therefore, the Al is usually placed on Cu using a near-infrared laser for Al-Cu lap welding. However, the laser absorption efficiency of metals also depends on temperature. As the temperature increases, the absorption efficiency rises slightly. Furthermore, in the keyhole-induced laser welding process, the absorption efficiency increases significantly when the melt metals are in a molten state and the multi-reflection of the laser in the keyhole. In addition, Cu has a laser absorption efficiency of around 60% at a wavelength of about 0.5 μm, which also offers new potential for Al-Cu dissimilar laser welding [33,62,63].

### 2.3. Brittle IMCs

Metals share the same crystal lattice, similar atomic radii, and adjacent periodic table positions, such as Cu and nickel (Ni), iron (Fe) and chromium (Cr). They can form an infinite solid solution during melting and solidification. Most metals don't meet these conditions and form finite solid solutions with a specific solubility, such as Fe and Al, Cu and Al, or even Fe and Mg, which are incompatible [64]. Finite solid solutions form low melting point eutectic and IMCs, and coarse crystals can lead to interfacial cracking. The brittle fracture will be produced due to thick IMCs that reduce the mechanical properties of the joint. Al and Cu are typical finite solid solutions, and the equilibrium phase diagram is shown in Fig. 4. Cu has the maximum solid solubility is only about 2.5 at. % in Al, while the maximum solid solubility of Al in Cu is 18.5 at. % [11]. As the laser irradiates the Al, the heat absorbed by the Al melts and evaporates, forming a keyhole and molten pool. However, the Cu below the Al absorbs a little heat causing only a small area of Cu to melt. During the melting process, metal atoms diffuse at the interface with the stirring and convection of the molten pool. Al and Cu elements begin to dissolve as they cool rapidly. Al solid solution precipitates when the temperature drops, IMCs (e.g., CuAl<sub>2</sub>,

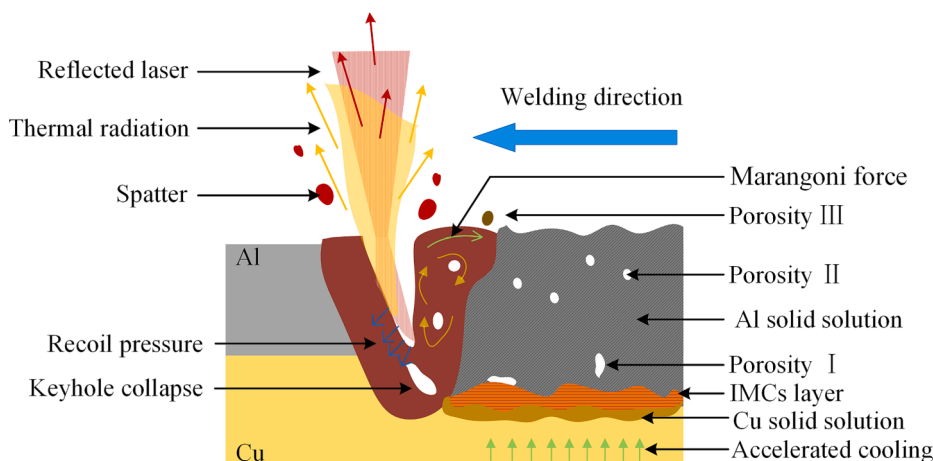


**Fig. 1.** Schematic diagram of the porosity formation in the Al-Cu laser welding process.

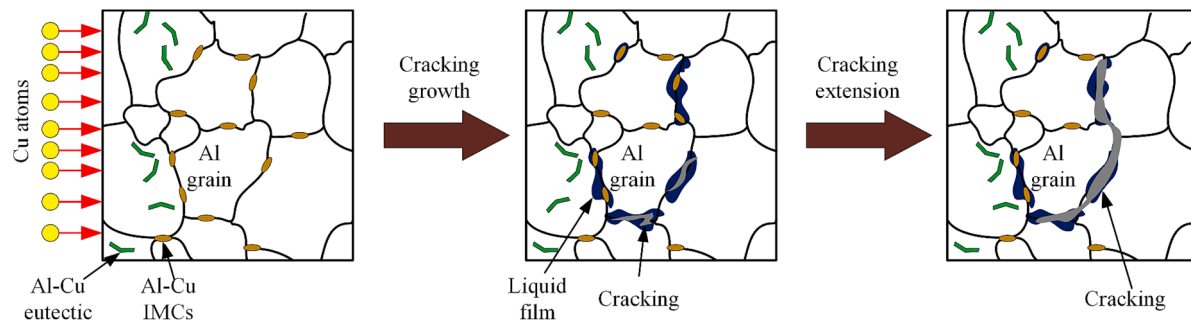


Fig. 2. Schematic diagram of the crack formation in Al-Cu joints.

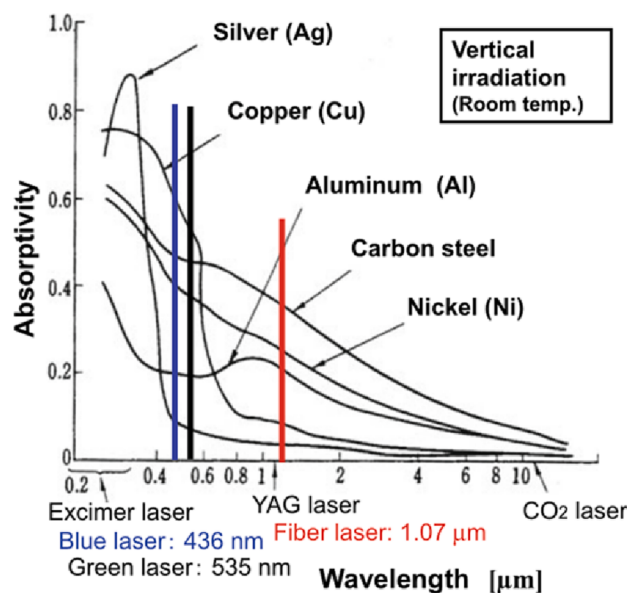


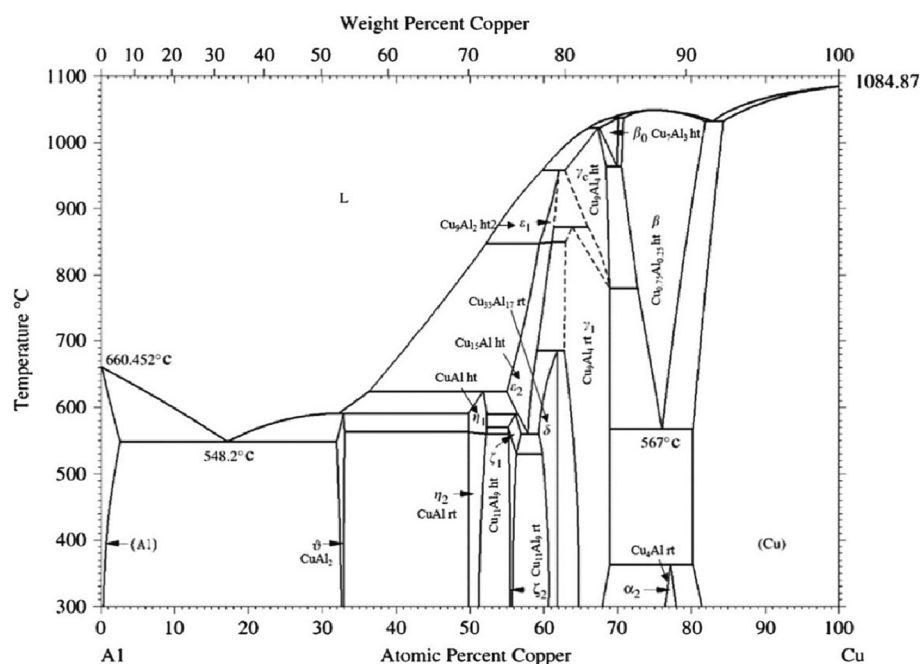
Fig. 3. Laser absorption efficiency of different metals [61].

CuAl, Cu<sub>9</sub>Al<sub>4</sub>, etc.) are easily precipitated in the fusion region where the average Cu concentration is higher than 50 wt% [37,40]. Continued cooling will produce Al-Cu eutectic, and the final solidification stage is the precipitation of a mixture of Al-Cu eutectic and Al solid solution [32].

The characteristic of Al-Cu IMCs is shown in Table 3, and they are primarily blocky and characterized by hard and brittle grain structures, whose electrical resistance and hardness are much higher than the base materials. The composition of the Al-Cu welded joint is shown in Fig. 5, which can be divided into four zones: Al solid solution, Al-Cu eutectic, Al-Cu IMCs, and Cu solid solution. As a result of Cu enrichment, the phases of  $\zeta$  (Al<sub>3</sub>Cu<sub>4</sub>) and  $\gamma$  (Al<sub>4</sub>Cu<sub>9</sub>) are formed in fewer amounts [68]. They are the hardest and most brittle IMCs, which are difficult to

**Table 3**  
Characteristic of Al-Cu IMCs [37,40,68].

Phase	Nominal composition [% at. Cu]	Chemical composition [% at. Cu]	Spec. Electrical resistance [ $\mu\Omega$ cm]	Hardness [HV]
(Al)	0–2.2	2.4	36	
0	Al <sub>2</sub> Cu	31.9–33	8.0	630
$\eta$	AlCu	51.9–54.8	11.4	905
$\zeta$	Al <sub>3</sub> Cu <sub>4</sub>	56–57.5	12.2	930
$\gamma$	Al <sub>4</sub> Cu <sub>9</sub>	64–69	14.2	770
(Cu)	80.3–100	2.0		75



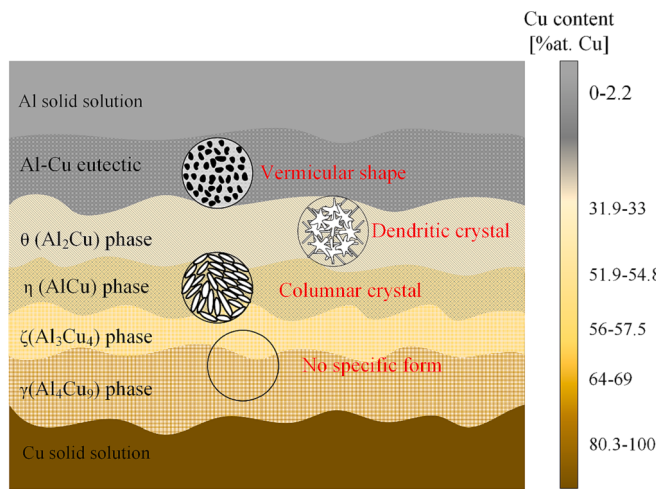


**Fig. 5.** Schematic diagram of the composition of Al-Cu welded joint.

identify in the Cu-rich region because they present as a Cu cluster without a specific form [74]. When the Al and Cu are mixed sufficiently during the welding process, a large amount of the  $\eta$  (AlCu) phase can be produced, and the crystal structure is columnar. Otherwise, it is found that the major phases of the Al-Cu joint near the Al base material are  $\theta$  ( $Al_2Cu$ ) and Al-Cu eutectic, which is in the form of dendrites and vermicular shape, respectively [32]. A certain thickness of IMCs can improve the joint's mechanical properties. However, if the thickness is greater than 2.5  $\mu m$ , joint strength decreases rapidly [12]. When greater than 5  $\mu m$ , the joint is susceptible to brittle fracture along that [66]. Thicker IMCs result in higher resistance of Al-Cu lug joints, intensifying the heat generation during charging and discharging and accelerating the battery degradation [37,40,67]. The phases of  $\gamma$  ( $Al_4Cu_9$ ) and  $\eta$  (AlCu),  $\zeta$  ( $Al_3Cu_4$ ) are harder and less ductile, which have a greater damaging effect on the joint in comparison with  $\theta$  ( $Al_2Cu$ ) [69].

The schematic diagram of the challenges, solutions, and functions of Al-Cu laser welding is shown in Fig. 6. In summary, the different material properties that make laser welding of Al and Cu with a higher crack sensitivity and poorer weldability. To overcome this, the optimal solution is adding filler metals or interlayers, which can form a transition zone to regulate the type of IMCs or reduce the metal mixing of Al and Cu to reduce cracking and the formation of brittle IMCs. The challenge of low laser absorption efficiency can be overcome by short wavelength laser, increasing the power energy density for keyhole welding, or changing the laser output mode to preheat the base material. The Al-Cu IMCs are inevitably produced in the laser welding process,

which can be reduced by decreasing the heat input or filling with transition metals to reduce the thickness of the IMCs or improve the type of IMCs. Different laser output modes, such as laser beam oscillation, pulse, and dual beam, are utilized to decrease susceptibility to cracking or porosity by reducing the temperature gradient of the molten pool in the laser welding process. All of the above possible solutions and their functions for Al-Cu laser welding are analyzed and discussed in detail in the following sections.

### 3. Laser welding process

The various factors affecting the joint quality of laser welding Al and Cu are shown in Fig. 7. Besides the above-mentioned physical and optical properties related to the base material, the quality of the Al-Cu laser welded joint is also influenced by the system parameters and the welding process parameters. Although laser welding of Al and Cu presents significant challenges due to the extensive material property differences and low laser absorption efficiency, the system and process parameters can be optimized to avoid or reduce welding defects and thus improve the weld quality. The beam quality is decided by the value of the beam parameter product (BPP). With smaller BPP, the beam quality is better. High beam quality lasers allow smaller spot diameter beams at the same lens focal length, achieving higher power density and thus deeper penetration or faster scanning speed. The defocus controls the spot diameter on the material's surface, affecting the laser power density. The laser transmission efficiency is most efficient when defocus amount is 0. The clamping force is a critical system parameter to ensure that laser welding can be performed correctly. Joint clamps include mechanical, pneumatic, hydraulic, and electromagnetic clamps. For laser welding of Al-Cu dissimilar metals, suitable clamps are required to meet two requirements: i. Ensure that there is no gap between the metal contact surfaces. ii. Ensure that the metal deforms the most minimally during welding and cooling. An inert gas such as Ar is typically used as shielding, which can protect the focusing lens from metal spatters. The molten pool will not oxidize during welding, reduce the weld porosity, and make the weld seam uniform and beautiful. Oxide films and stains on the surface of the base material can cause weld inclusions and porosity, which must be polished and cleaned before laser welding. The key parameters are laser welding parameters, lap methods, and laser output modes. These parameters affect the weld width of Al-Cu joints, weld penetration, microstructure, and mechanical or electrical properties, which are discussed in detail in the following sections.

#### 3.1. Laser welding parameters

The laser power, scanning speed, and spot diameter determine the

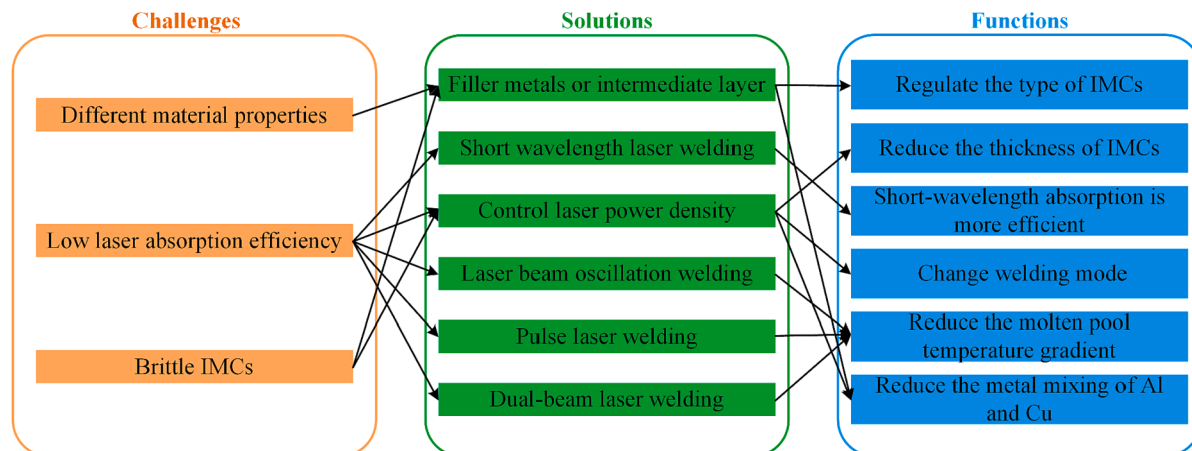


**Fig. 6.** The schematic diagram of the challenges, solutions, and functions of Al-Cu laser welding.

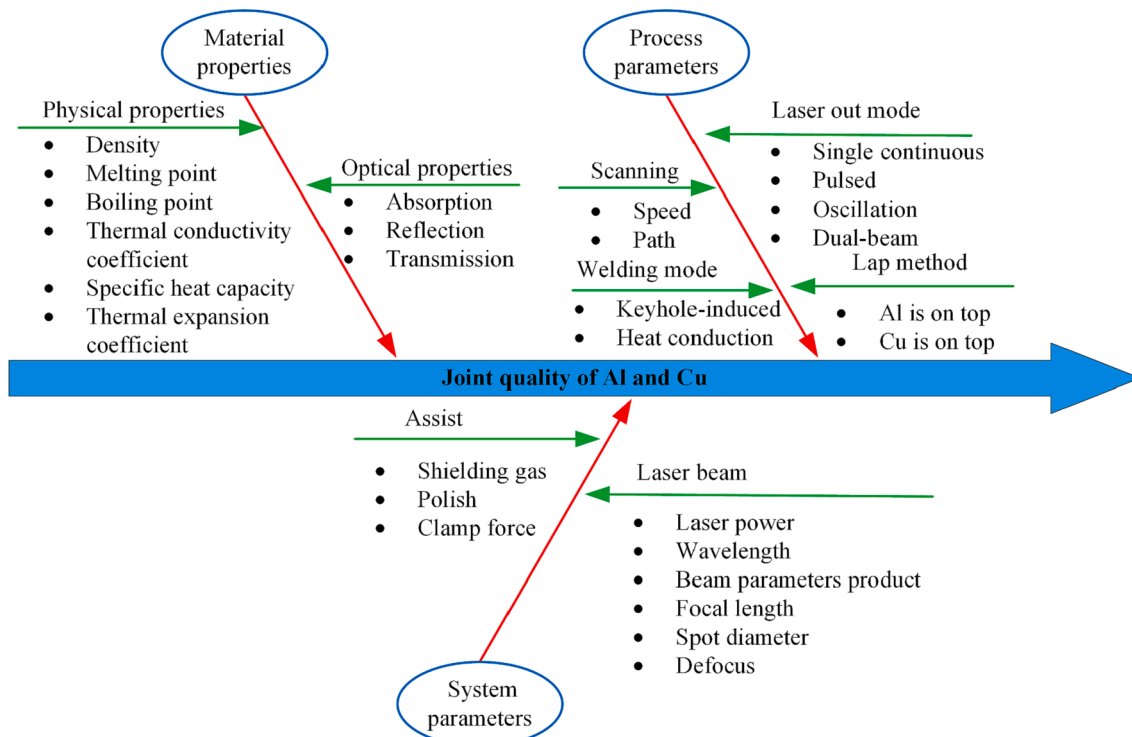


Fig. 7. The various factors affecting the quality of Al-Cu laser welded joints.

power density input. The low power density is insufficient to melt Al and Cu, resulting in incomplete fusion defects. When it is high enough, the diffusion of molten metal atoms is facilitated, leading to the formation of IMCs. It is necessary to adjust and optimize the process parameters to require an appropriate power density and to balance IMCs and mechanical strength. The laser power and welding speed determine laser heat input at a constant spot diameter, expressed in line energy. The effect of laser power on resistance properties, mechanical properties, IMC layer, and hardness of Al-Cu joints is shown in Fig. 8 [70]. The laser power determines the potential energy absorbed by the molten pool, which is increased to melt penetrate the top Al (Cu) layer and react metallurgically with the Cu (Al) combination. Higher laser power means that more metal is melted, which promotes intense interdiffusion between Al and Cu and thus increases the formation of IMCs, resulting in harder joints, increased resistance, brittle joints, and reduced

mechanical properties. Yan et al. [32] also confirmed that the tensile strength of the Al-Cu joints (6061 Al and pure Cu are all 1.6 mm thick) increased and then decreased with increasing laser power. The maximum tensile strength of about 99.8 MPa was obtained at 2.45 kW laser power and 2 m/min welding speed. In addition, the laser power also affects the microstructure of the joint interlayer. An increasing laser power leads to an increasing primary dendrite arm spacing and the growth of secondary dendrite in the hypoeutectic zone [71]. The welding speed determines the time the laser interacts with the material. As the welding speed increases, the laser welding mode can be changed from keyhole induction to heat conduction, reducing Al and Cu mixing and forming IMCs [72].

As shown in Fig. 9, the metal mixing is determined by combining the recoil pressure at the keyhole bottom and the Marangoni stress at the molten pool [73]. Under the effect of recoil pressure, the Cu at the bottom moves toward the surface of the molten pool. And the Marangoni stress causes the metals to form a vortex mixing pattern. Increasing the laser power increases both the recoil pressure and the Marangoni stress to drive more Cu to migrate upward and mix with Al. Increasing the welding speed results in a shorter laser heating time, which contributes to a shorter acceleration time of the local fluid by the laser-induced recoil pressure, thus reducing the fluid flow rate and Cu concentration. When the line energy is constant, combining high power and high-speed parameters allows more Cu to move up and mix with Al, forming more IMCs.

The schematic diagram of the effect of laser welding parameters on Al-Cu joints' mechanical and electrical properties is shown in Fig. 10. The laser power density (power/welding speed/spot diameter) plays a role in the Al-Cu joint strength. The material's high reflection and thermal conductivity require high-power density to form an effective joint. However, excessive laser heat input can increase the mixing of Al and Cu in the molten pool, thus promoting the formation of IMC. The thicker IMC layer harms the joint's mechanical strength and electrical properties, which must be avoided in Al and Cu laser welding. As mentioned above, reducing the laser power or increasing the welding speed can reduce the mixing of metals. However, insufficient power

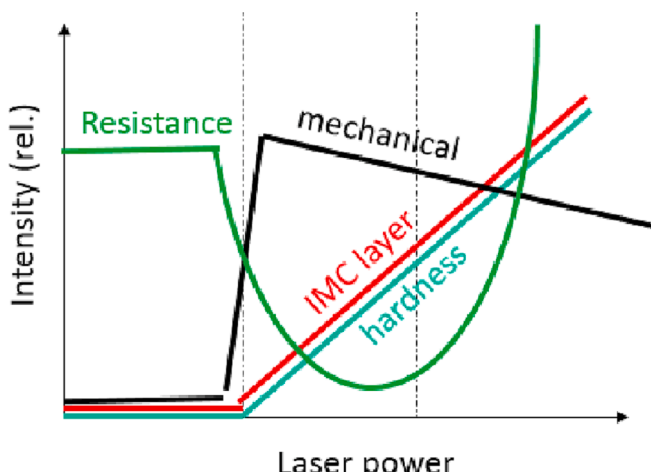
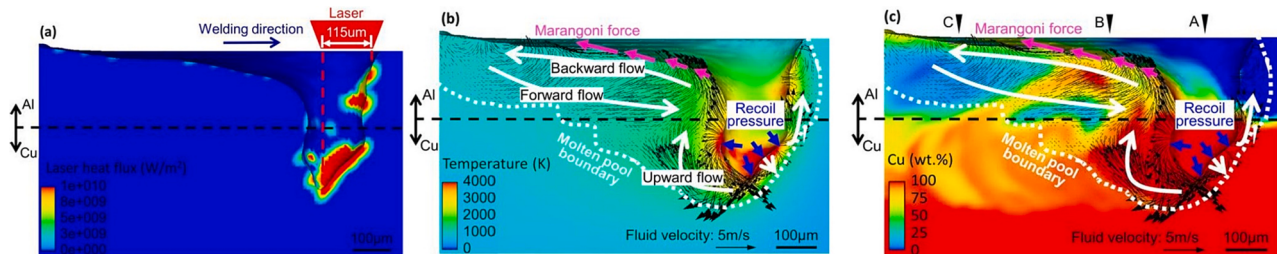
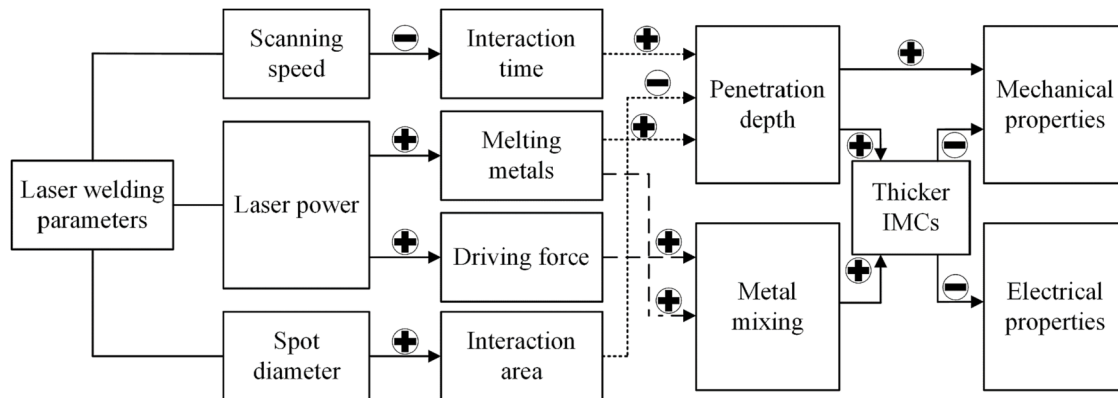


Fig. 8. Effect of laser power on resistance properties, mechanical properties, IMC layer, and hardness of Al-Cu joints [70].



**Fig. 9.** Simulation results of the longitudinal section views of Al-Cu joints [73]. (a) Laser heat flux field. (b) Temperature and fluid velocity fields. (c) Cu concentration field.



**Fig. 10.** Schematic diagram of the effect of laser welding parameters on Al-Cu joints' mechanical and electrical properties. (⊕: positive. ⊖: negative).

density can also easily lead to unfused defects. To ensure sufficient power density and reduce the mixing of metals, a smaller spot diameter is the key to optimizing the welding process. A smaller spot diameter allows for lower laser power and higher welding speed while maintaining sufficient power density to be absorbed by the material, which provides a more comprehensive process window to decrease the thickness of the IMCs layer and increase the mechanical strength and electrical properties of the joint [74]. However, the small spot diameter reduces the interaction area so that the tensile force of the joint is weak. On this basis, laser beam oscillation or high-frequency pulsed laser is applied to design different scanning trajectories to increase the joint area and avoid the defect of low tensile force caused by small spot diameter.

### 3.2. Lap method

The different lap methods (Al is on top or Cu is on top) can also affect the joint quality of Al and Cu due to their different material properties and laser absorption efficiencies. The schematic diagram of different lap methods for Al-Cu laser welding is shown in Fig. 11. Because the Cu has a higher melting point, the interface temperature of Al being on top is not enough to melt the bottom plate of Cu, and the melting penetration depth is lower than that of Cu being on top when the heat input is the same. However, micro-segregation and metal interatomic reactions during solidification should be addressed. The poor fluidity of molten Al makes the atoms' diffusion weak when Al is on top, resulting in an intermediate layer with a lower thickness than Cu on top [75]. When Cu is on top, it is more likely to diffuse downward because of its higher density, which makes it easier to form IMCs when Cu elements are entirely distributed in Al. The interface is easy to create a Cu-rich zone to

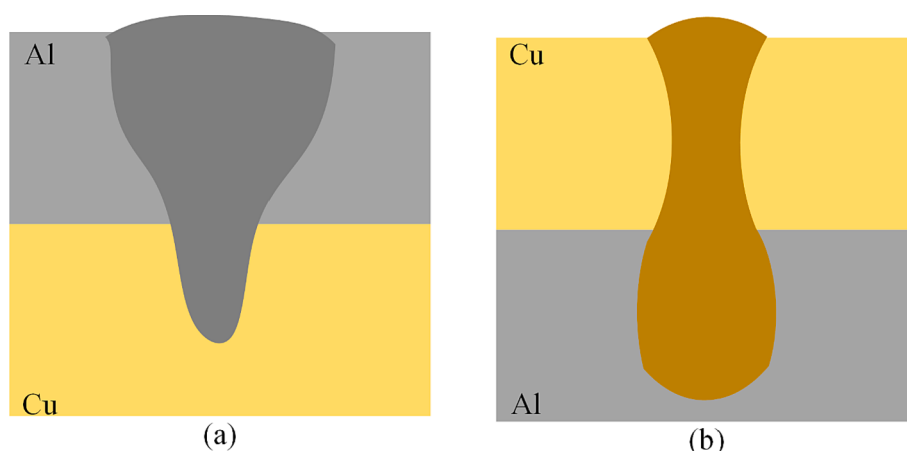


**Fig. 11.** The schematic diagram of different lap methods for Al-Cu laser welding. (a) Al is on top. (b) Cu is on top.

precipitate the IMC phase during solidification. When Al is on top, the interface contact zone narrows, forming a thin IMCs layer with excellent electrical conductivity [72,76]. Therefore, the cross-section of Al-Cu joints is funnel-shaped and bottle-shaped at different lap methods. In laser beam oscillation, amplitude significantly affects the aspect ratio of the lap joint when Al is on top. But has little effect when Cu is on top due to the molten Al's poor fluidity [34].

### 3.3. Laser output mode

A single continuous laser causes an unstable keyhole and molten pool due to the high energy density and smaller heat-affected zone [77]. Especially in welding Al and Cu, poor fluidity of the molten Al and the rapid cooling rate (caused by Cu's excellent thermal conductivity) lead to spatters in the welding process and porosity or cracking in the weld joint, which cannot be avoided by optimizing the process parameters. To address this issue, different laser output modes such as beam oscillation, pulsed and dual-beam hybrid have been designed to improve temperature gradients and molten pool. Their applications and mechanism in laser welding of Al/Cu are discussed as follows.

Laser beam oscillation is achieved by a fiber laser in combination with a galvanometric scanning head equipped with an F-Theta lens. The oscillation parameters are adapted to the gap size to produce sufficient molten material and increase the molten pool width and dynamics [78,79]. As shown in Fig. 12, laser beam oscillation allows for a uniform distribution of heat input. It reduces the temperature gradient, enlarging the supercooling zone at the center of the weld [54]. The grain structure and size of the weld can be affected by changing the temperature gradient ( $G$ ) and solidification rate ( $R$ ). The value of  $G/R$  determines the grain morphology, and  $GR$  determines the grain size. Compared to single laser welding, the effect of temperature gradient and solidification rate of the laser beam oscillation welding on the grain structure of the joint is shown in Fig. 13. The weld width of laser beam oscillation is wider. Its solidification rate from the weld centerline to the fusion boundary tends to decline more slowly. At the same distance from the weld's centerline, the beam oscillation's solidification rate is greater than that of single laser welding. Therefore, the laser beam oscillation with a lower value of  $G/R$  and  $GR$  promotes equiaxed grain growth with larger grain size [80,81]. In addition to affecting the tensile strength and ductility of the joint, the grain structure and size of the weld have a significant relationship to the susceptibility of the joint to thermal cracking [82]. Due to the relatively small diameter of the equiaxial crystals, a large number of grain boundaries are created in the weld, which reduces the susceptibility to thermal cracking due to the spreading of the thermal stress

across multiple grain boundaries during the solidification of the material. On the other hand, oriented dendrites with elongated shapes exhibit large grains and a single continuous grain boundary in the single laser welding joint, making them especially susceptible to cracking [54].

Laser beam oscillation combines transverse periodic oscillation and longitudinal uniform linear motion. The longitudinal oscillation increases the area of the material surface that absorbs laser radiation [83]. The oscillation parameters can be adapted by amplitude and frequency. As shown in Fig. 14, the share of Cu in the fusion zone is linearly related to the welding depth. The high amplitude can decrease the penetration depth and form a tooth-shaped cross-section. But the oscillation frequency has little effect on penetration depth [84]. Low penetration depth means less mixing of Al/Cu, resulting in a lower thickness of IMCs with no cracks at the interface. However, increasing the oscillation amplitude at the same energy density favors mixing metals and the thicker IMC in the form of the AlCu phase with columnar crystals, leading to brittle fracture and reducing the maximum fracture load [85].

Pulsed laser welding can be considered a series of pulse spot welds. In contrast to continuous laser welding, the heat input from pulsed laser welding is determined by a combination of the peak power, pulse width, and pulse frequency. As shown in Fig. 15, the pulsed laser is a stationary weld, and the formation of the keyhole is mainly caused by the surface tension due to the molten pool temperature gradient [86]. And the Marangoni effect induces the circulation of the molten pool, mixing Al and Cu and forming swirl-like structures at the Al-Cu joints [13]. The spot overlap effect can reduce the temperature gradient, thus reducing the formation of cracks and pores in Al/Cu pulsed laser welding joints.

The low-frequency pulsed laser can adapt the output energy by adjusting the different pulse shapes. As shown in Fig. 16 (a), the pulse shape was defined by the phases of preheating (PH), active welding (AW) time, and cooling (CL) within the pulse width [87]. At the same power density, a pulse shape with a PH phase can increase the laser absorption and reduce the temperature gradient at the molten pool, producing better mechanical strength results than pulse shapes with high initial peak power [14,88]. As shown in Fig. 16 (b), the absence of the PH stage makes pulse B more likely to result in porosity relative to A. As the AW time increases, interdiffusion and defects such as porosity and cracks occur.

High-frequency pulsed lasers have a defined pulse shape and lower energy per pulse (typically less than 100 W) than low-frequency pulsed lasers. Due to their high beam quality and minimal spot diameter, high-frequency pulsed lasers can be designed with various scanning paths for spot and seam welding. In addition to laser marking and etching, high-frequency pulsed lasers are increasingly used to micro-connect thin

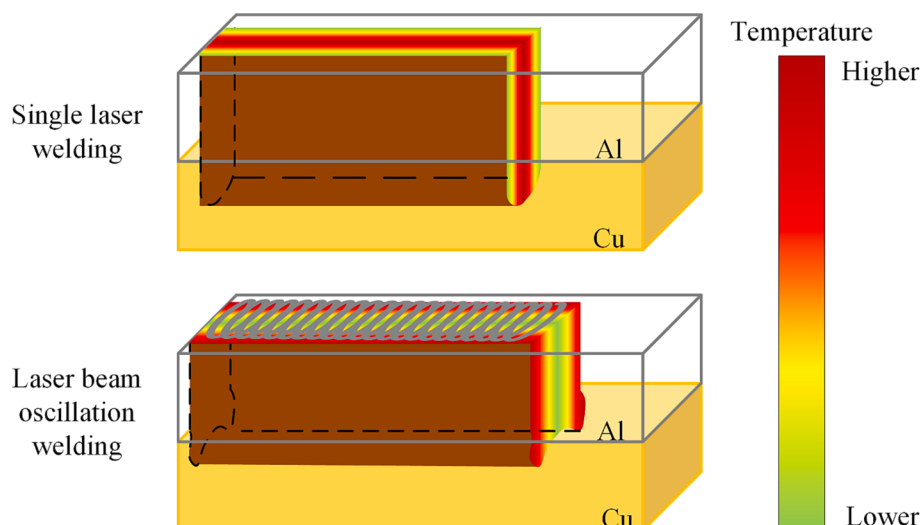
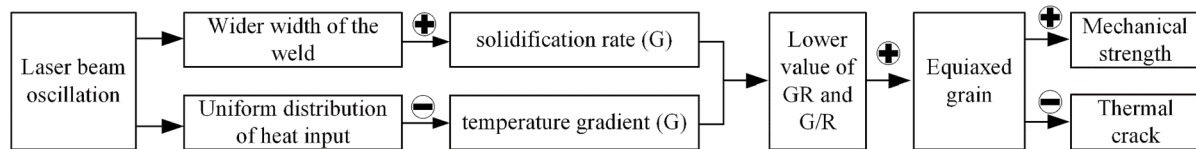
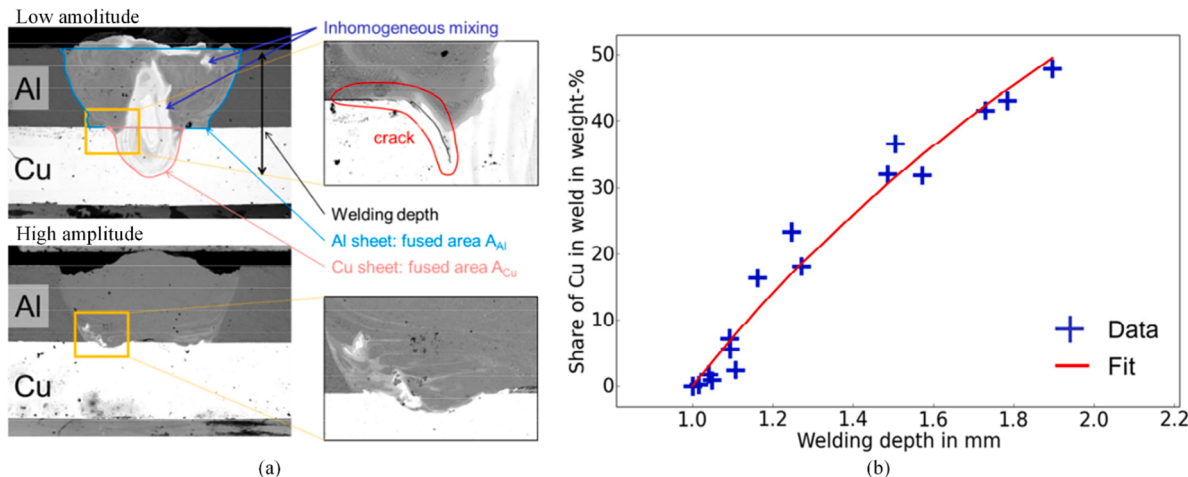


Fig. 12. Laser energy distribution of beam oscillation and single laser.



**Fig. 13.** Schematic diagram of the effect of temperature gradient and solidification rate on the grain structure of the joint for laser beam oscillation welding. ( $\oplus$ : positive.  $\ominus$ : negative).



**Fig. 14.** Laser beam oscillation welding of Al and Cu [84]. (a) Cross sections under different oscillation amplitude. (b) Share of Cu in the fusion zone on the welding depth.

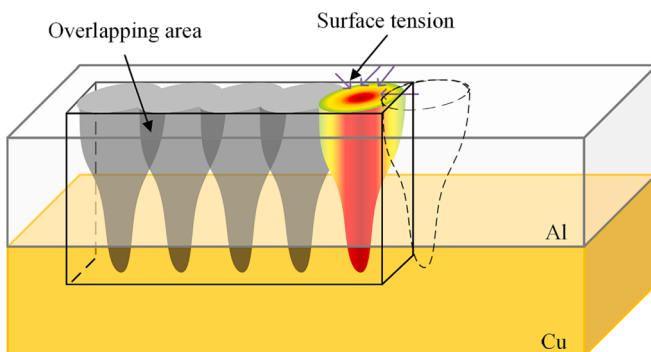


**Fig. 15.** The schematic diagram of Al-Cu pulse laser welding.

sheet metals. Fig. 17 shows the different scanning paths employed to laser spot welding Al/Cu [89]. The weld in the outer spiral forms a tooth-like structure, enhancing the mechanical bonding. In contrast, concentric circle and straight welded joints produce large pores and cracks caused by the heat accumulation process during welding. Of course, the effect of the distance of the outer spiral scanning on heat accumulation cannot be ignored [90].

Whether a high-frequency pulsed laser or a low-frequency pulsed laser, the spot diameter was the key to overcoming Al and Cu's high reflection and thermal conductivity [91]. The smaller spot diameter results in a more comprehensive process window and reliable control. Due to the spot overlap effect, different pulsed laser sources positively reduce porosity and cracking. However, excessive heat input lead to a higher mixing of the base metals, promoting brittle IMC formation. Compared with single-mode continuous laser, laser oscillation mode, and laser pulse mode can effectively suppress the defects such as porosity and cracks generated by the Al-Cu laser welding process and also reduce the mixing of Al and Cu to control the thickness of IMCs layer to a certain extent. In addition, it brings the problem of optimization

difficulties because of the large number of process parameters. By employing experimental and numerical simulations, Tien et al. [92] investigated the optimal process parameters for multi-parameter oscillating pulse laser welding of Al-Cu joints. The numerical simulation was employed to predict the molten pool geometry and Cu concentration for different parameter combinations, and the results were trained and experimentally verified according to quality standards to determine the best combination of parameters with no defects and the best mechanical and electrical properties.

The dual-beam laser, a new hybrid laser heat source, has been developed to improve the stability of the keyhole and molten pool during laser welding. As shown in Fig. 18. The laser integrates two concentric inner and outer near-infrared wavelengths to concentrate light: a low-power density ring laser outside and a high-power density circular Gaussian laser inside. The hybrid laser can control the laser power of the core beam and the ring beam separately. Compared to single laser beam welding, it can change the energy distribution of the laser irradiation to control the surface solidification rate and stabilize the keyhole to reduce spatters and improve the weld quality [93–95]. Beams at different locations have different roles in the welding process. The front of the ring can play a role in preheating the weld, the middle of the ring and the center of the Gaussian laser is the key to the formation of the keyhole, and the rear of the ring plays a post-heating role. The center and ring can remove pores, and the gap between the ring and center can stable keyhole conditions [96]. In addition, the dual-beam laser can remain the keyhole stably open, which significantly reduces the difficulty in locating the measurement beam when utilizing the OCT (optical coherence chromatography) technique for real-time detection of Al-Cu weld depth and improves the accuracy of about 50% compared to single laser beam welding [45].

The effect of various process parameters on the quality of Al-Cu laser welding is comprehensively summarized in Fig. 19, and Table 4 summarizes research conducted on laser welding of Al and Cu. During laser welding of Al and Cu, the metal vapor's recoil pressure and the molten pool's vortex flow inevitably lead to the mixing of Al and Cu, forming

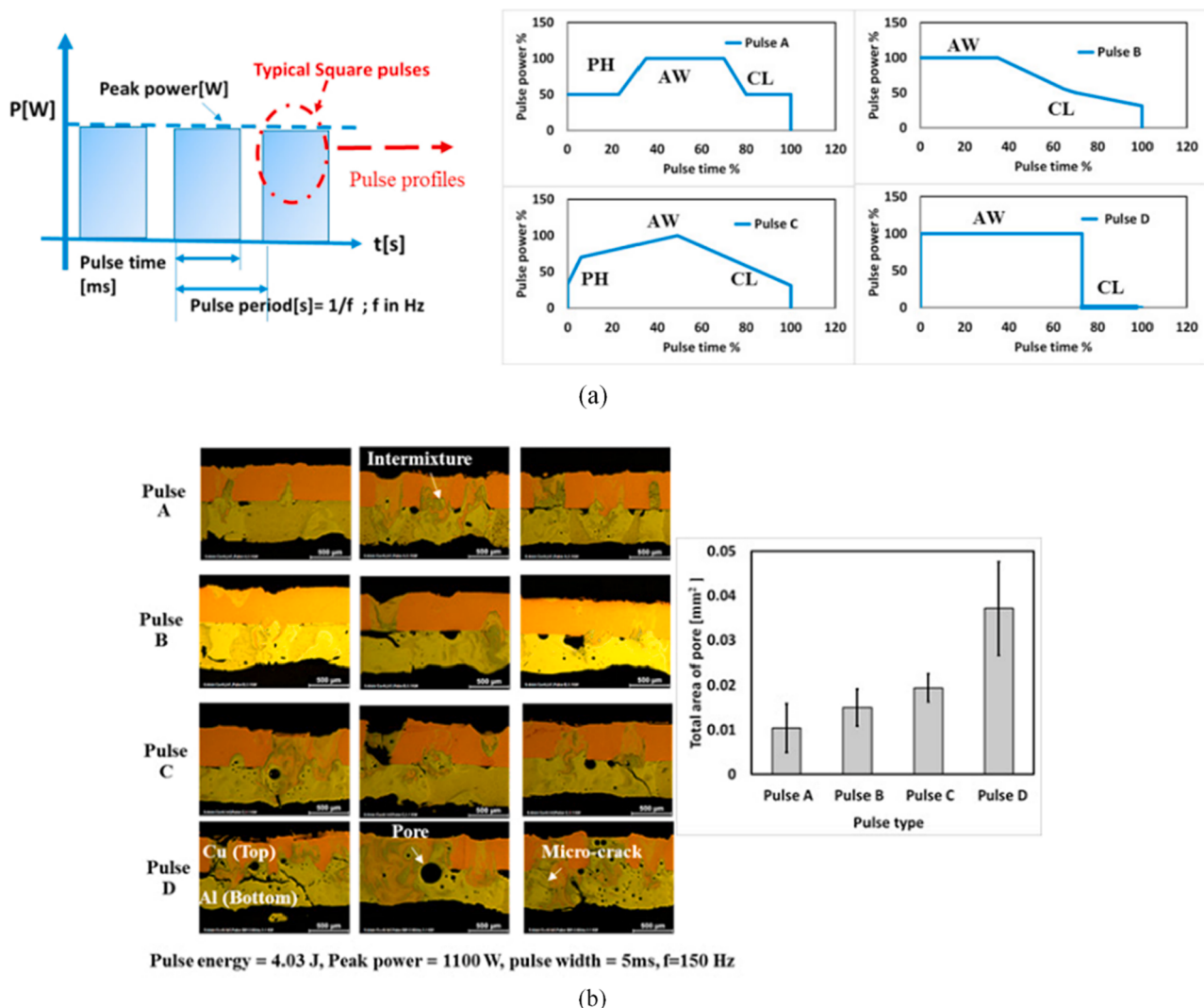


**Fig. 16.** Different pulse shapes and their micrographs in welding Al and Cu [87]. (a) Different pulse shapes. (b) Micrographs of Cu-Al joint's cross-sections.

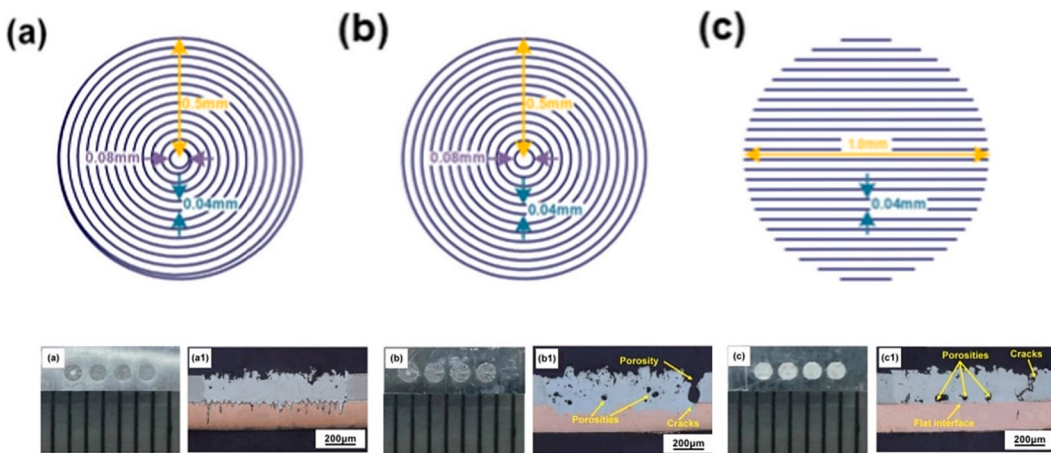


**Fig. 17.** Different scanning paths and weld appearances during the nano-second pulse laser welding of Cu to Al [89]. (a) Outer spiral. (b) Concentric circle. (c) Straight.

the brittle IMCs. The various process parameters affect the penetration depth and IMC thickness mainly through the magnitude of the laser power density and the degree of metal mixing, thus affecting the mechanical and electrical properties of the joint. Also, different lap

methods or welding modes can affect the welded joint differently depending on material properties and the laser absorption efficiency. Due to the poor fluidity of Al, hard and brittle IMCs, and thermal cycling, single laser beam welding of Al and Cu is highly susceptible to cracking

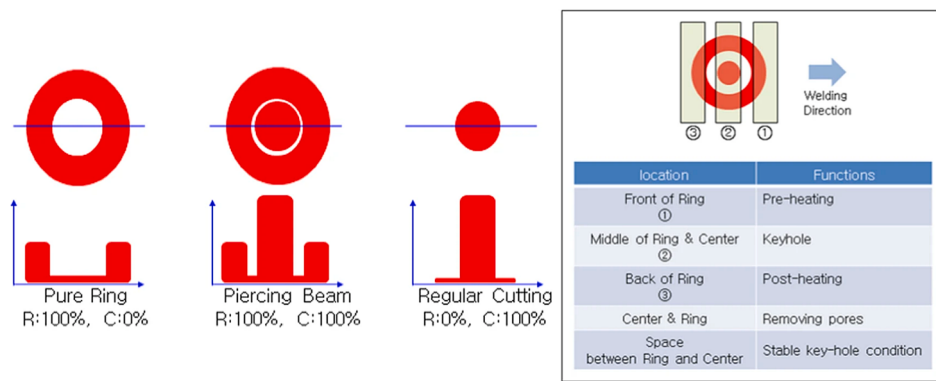


Fig. 18. The schematic diagram of dual-beam laser [96].

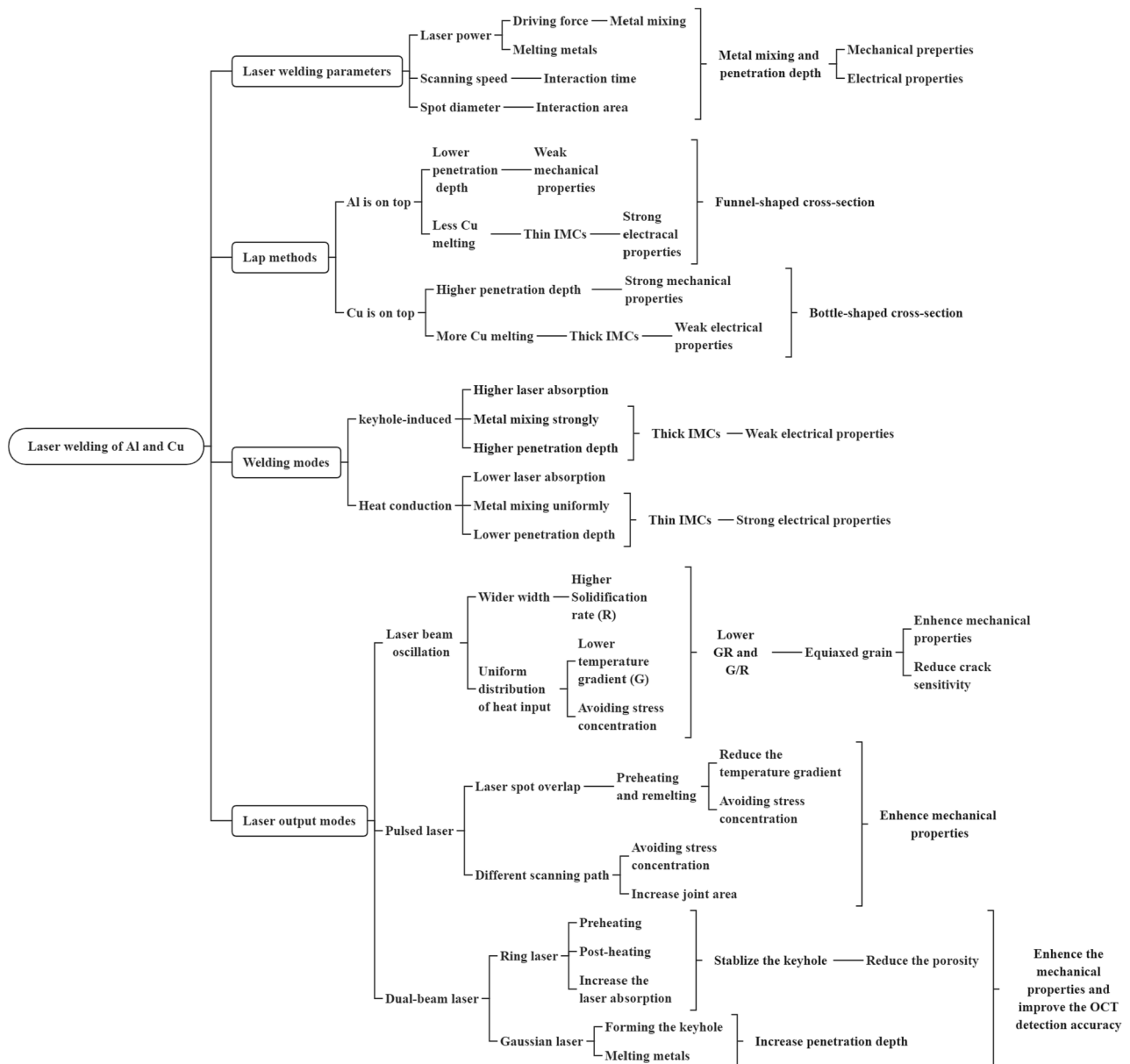


Fig. 19. The schematic diagram of the effect of various process parameters on the quality of Al-Cu laser welding.

**Table 4**

Summary of research conducted on laser welding of Al and Cu.

Material		Laser welding process parameters					Results			Refs
Type	Thickness (mm)	Laser type	Lap method	Spot diameter ( $\mu\text{m}$ )	Power (kW)	Welding speed (mm/s)	Mechanical strength	Electrical property	Major IMCs	
1050 Al-pure Cu	0.45Al 0.3Cu	CLW	Cu-Al	A: 68 B: 175	A: 0.6–1 B: 1–1.5	A: 150–250 B: 150–250	A: 650–750 N B: 750–900 N	A: 42–45 $\Omega$ B: 40–47 $\Omega$	AlCu Al <sub>2</sub> Cu Al <sub>3</sub> Cu <sub>4</sub> Al <sub>4</sub> Cu <sub>9</sub> Unknown	[74]
AA1100 Al-C10100 Cu	0.2 Al 0.5Cu	CLW	Al-Cu	115	0.668–1.17	200–350	Unknown	Unknown	Unknown	[73]
6061 Al-110Cu	1.6 Al 1.6 Cu	CLW	Al-Cu	Unknown	2–3.35	33.33	Max 99.8 MPa	Unknown	Al <sub>2</sub> Cu	[32]
1060 Al-T2 Cu	Unknown	CLW	Al-Cu	400	1.45–1.85	100	Unknown	Unknown	AlCu Al <sub>2</sub> Cu	[71]
1050 Al-pure Cu	0.3	CLW	A: Cu-Al B: Al-Cu	20	1	83.3–833	A: 50–205 MPa B: 30–160 MPa	Unknown	AlCu Al <sub>2</sub> Cu Al <sub>4</sub> Cu <sub>9</sub>	[72]
1060 Al-T2 Cu	0.2	PLW	A: Al-Cu B: Cu-Al	Unknown	0.07	A: 120 B: 70	A: 53.5 N/mm <sup>2</sup> B: 79 N/mm <sup>2</sup>	Unknown	AlCu Al <sub>2</sub> Cu Al <sub>4</sub> Cu <sub>9</sub>	[76]
Al 99.5-oxygen-free Cu	1	LBO	Al-Cu	280	3.25	100	Unknown	Unknown	Unknown	[84]
1050 Al-oxygen-free Cu	0.6	LBO	Cu-Al	89	0.95–1.8	50	600–1800 N	Unknown	Unknown	[83]
99.99% Al-99.9% Cu	0.2 Al 1 Cu	PLW	Al-Cu	200	1.8–3	10–40	Max 33.5 MPa	261–372 $\Omega$	AlCu Al <sub>2</sub> Cu Al <sub>3</sub> Cu <sub>4</sub> Al <sub>4</sub> Cu <sub>9</sub>	[13]
1050 Al-99.95%Cu	0.4	PLW and LBO	Cu-Al	89	0.6	30	1222–1275 N	Unknown	AlCu Al <sub>2</sub> Cu Al <sub>3</sub> Cu <sub>4</sub> Al <sub>4</sub> Cu <sub>9</sub>	[87]
1050 Al-1020 Cu	0.45 Al 0.3 Cu	PLW	Al-Cu	635	0.2	2.4–28.8	Max 120 kgf	Min k factor 1.01	Unknown	[88]
Pure Al-99.99%Cu	0.25 Cu	PLW	Cu-Al	300	Unknown	Unknown	Max 231 MPa	Unknown	Unknown	[14]
6063 Al-pure Cu	0.2	PLW	Al-Cu	Unknown	0.07	50	Max 63.05 MPa	Unknown	Al <sub>2</sub> Cu Al <sub>2</sub> Cu <sub>3</sub>	[89]
6063Al-T2 Cu	0.4 Al 0.2 Cu	PLW	Cu-Al	Unknown	0.07	30	Max 107.7 N	Unknown	Al <sub>2</sub> Cu	[90]
AA1050 Al-C1020 Cu	0.2 Al 1 Cu	PLW	Al-Cu	30	0.45–0.89	242–702	408–1209 N	86–133 $\mu\Omega$	AlCu Al <sub>2</sub> Cu Al <sub>3</sub> Cu <sub>4</sub>	[92]
6061 Al-C102P Cu	0.4	ARM	Al-Cu	Core 70 $\mu\text{m}$ Ring 180 $\mu\text{m}$	Core: 0.82–0.9 Ring: 0.7	200	Max 55 MPa	Unknown	Unknown	[96]
1050 Al-Pure Cu	0.45 Al 0.3 Cu	ARM	Al-Cu	Core 140 $\mu\text{m}$ Ring 360 $\mu\text{m}$	Core: 0.65 Ring: 0.05–1.5	175	Unknown	Unknown	Unknown	[45]

CLW-Continuous laser welding; PLW-Pulse laser welding; LBO-Laser beam oscillation; ARM-Adjustable ring mode.

and porosity. The different laser output modes can remelt and solidify the fusion zone to reduce the molten pool temperature gradient, improve the grain structure of the joint and reduce the formation of cracks and porosity, and improve the mechanical properties using beam oscillation, pulsed laser spot overlap, and dual-beam laser, respectively.

#### 4. Filler metals

Large deviations in the physical properties of Al and Cu and their poor metallurgical affinity result in high crack sensitivity and the formation of brittle IMC phases during the welding process. Although optimization of the welding process and control of the heat input can reduce defects and thickness of the IMC layer, direct contact between Al and Cu cannot be avoided. As a solution, filler metals with a strong chemical affinity for Al/Cu dissimilar metals are selected to prevent direct contact and control the type or thickness of the IMCs layer. The filler metals can effectively reduce the excessive mixing of Al and Cu in the molten pool and metallurgically react with the base material to form a transition zone to reduce thermal cracking. Pure metals such as silver (Ag), tin (Sn), Ni, and silicon (Si) adjacent to base materials in the periodic table and their multi-element alloys feature comparatively good compatibility with copper and aluminum and effectively reduce the melting of base materials [97]. Thus, the type of IMCs could be improved to enhance the welding quality of the Al-Cu joint.

#### 4.1. Pure metals

The pure metals (Ag, Ni, and Sn) as fillers significantly improve the static and dynamic mechanical stability of Al/Cu joints and adequately control the volume fraction of Cu and Al. Filler metals in the fusion zone help to avoid material segregation and reduce residual stresses, thus reducing crack affinity and stabilizing electrical properties [98,99]. It was found that Ag foil had a significant effect on the mechanical properties of Al-Cu welded joints, whose mechanical strength reached 800 N when the thickness of the Ag foil reached 100  $\mu\text{m}$ . The mechanical properties of the joints were related to the thickness of filler metals. The thickness of electroplated Ni had almost no effect on the tensile strength of the joint below 3  $\mu\text{m}$ , and the mechanical strength improved significantly only when it reached 10  $\mu\text{m}$ . The addition of interlayer filler metals improves the welding performance of Al-Cu dissimilar metals and the mechanical and electrical contact properties of the joint.

Ni and Cu are infinite solid solutions and do not produce IMCs during melting and solidification. But Al and Ni are finite solid solutions and yield IMC of AlNi. Ni has a low thermal conductivity and can inhibit heat diffusion from Al to Cu to reduce the melting of Cu, but this also increases the heat absorbed on the Al side and increases the melting of Al. Based on these studies, many scholars have utilized Ni as a filler metal for Al-Cu laser welding to improve the mechanical properties of the joint. The effect of the Ni interlayer on Al-Cu joints was investigated by Furuya et al. [100]. Adding Ni foil could enhance the mechanical strength of Al-Cu joints due to the formation of (Cu, Ni) Al interlayer

between  $\text{Al}_2\text{Cu}$  and  $\text{Al}_4\text{Cu}_9$  in the IMCs layer. Adding filler metals increases the thickness of the interlayer, but they can dissolve with Cu without a chemical reaction, and the thickness of the IMCs does not increase compared to that without the filler metals [69].

To prevent excessive diffusion and the reaction of Al and Cu in the laser welding process, Yan et al. investigated the effect of Ni interlayer on the interfacial structure composition and mechanical properties [101]. The joint's width and penetration depth increased gradually with increasing laser power, and Ni had little effect. At low power, the molten Al preferentially reacts with the Ni atoms to produce  $\text{AlNi}$  IMC, and no  $\text{Al}_2\text{Cu}$  IMC is produced. With the increase of laser power, more Cu started to melt and diffuse into the melt pool to react and consume the molten Al, and more  $\text{Al}_2\text{Cu}$  was formed before the melt pool solidified. The highest content of  $\text{AlNi}$  was observed when the laser power was up to 2.9 kW. As the laser power increased, more Cu melting reacted with Al causing the  $\text{AlNi}$  content to decrease. As shown in Fig. 20, a thinner  $\text{Al}_2\text{Cu}$  IMC layer with a sawtooth shape can potentially suppress the thermal stresses through the laser welding process, but the Ni interlayer inhibits the reaction of Al and Cu, resulting in increased susceptibility to cracking in the joint. Therefore, the appropriate heat input must be adjusted to balance IMC and thermal cracking.

#### 4.2. Sn-based alloys

Hailat et al. used 100  $\mu\text{m}$  thickness tin alloy (Sn–Ag–Ti) as a filler metal to enhance the compatibility of Al and Cu [102]. It was attributed to the Al–Ag–Cu alloy formation, which reduced Al and Cu mixing. The tin alloy acts as an intermediate layer absorbing part of laser energy and forming a heat transfer resistance to reduce the penetration depth. The results show that adding tin alloy improved Al distribution's uniformity, causing a uniform fracture shape and less fracture damage. However, as shown in Fig. 21, the Al–Cu joint with tin alloy is always accompanied by the formation of porosity inside the Al. There was no specific explanation for this phenomenon, and it was speculated that adding tin alloy tends to cause a collapse of the Al side keyhole or the rejection of hydrogen from the solid phase in the welding. The mechanical strength was not affected since the fracture in the tensile shear test occurred away from the porosity.

$\text{Al}_2\text{O}_3$  films on the Al substrate surface isolate the contact between the Sn-based filler metal and the Al substrate, resulting in poor wettability. Huan et al. improved the wettability of Sn-based (Sn–3Ag–0.5Cu) filler metals by Ni plating of Al substrate [103]. As shown in Fig. 22, the Ni plating layer and Sn-based filler metal avoided forming Al–Cu IMCs. The joint interlayer consisted mainly of  $\beta$ -Sn dendrites and  $\text{Ag}_3\text{Sn}$ , and the  $\text{Cu}_6\text{Sn}_5$  and  $(\text{Cu}, \text{Ni})_6\text{Sn}_5$  were created at the Cu side and Ni interlayer, respectively. The fracture of laser welded joints occurred along the brittle  $(\text{Cu}, \text{Ni})_6\text{Sn}_5$  IMC formed at the Ni layer interface, and the fracture mode was dominated by ductile fracture.

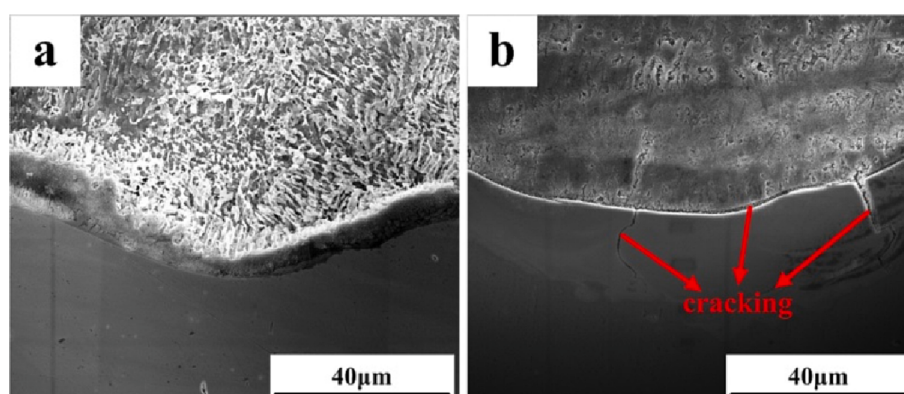


Fig. 20. The microstructure of the Al–Cu interface [101]. (a) Without Ni foil. (b) With Ni foil.

#### 4.3. Zn-based alloys

The Zn element in Zn-based filler metals readily reacts with Cu to form the brittle Zn–Cu IMC. Lei et al. found that Zn-based (Zn–Al) filler metals have better wettability compared to aluminum, that Zn elements can react with copper to form new IMCs ( $\text{CuZn}$  and  $\text{CuZn}_5$ ), thus effectively preventing the diffusion of copper atoms, and that the new brittle phase has better mechanical properties compared to the Al–Cu brittle phase [38]. However, in Zhu's study, Zn–Cu IMCs were detrimental to the mechanical strength of Al–Cu joints, and the Zn–Cu IMCs were avoided by adding tin foil and Ni layer in the presence of Zn-based filler metal [35]. Tin foil had little effect on the joint strength and significantly improved the diffusion and wetting ability of the filler metal but weakened the bond between the joint and the Al base material. Ni coating had a significant strengthening effect on the Al–Cu joint, and the diffusion of Cu was limited by the Ni coating and the mutual attraction between Al and Ni atoms, forming a Zn–Ni–Al ternary phase replacing the brittle Zn–Cu IMCs. The mechanical strength was increased by 15.5% compared to that without an interlayer.

#### 4.4. Si-based alloys

The Si element can lead to a lower viscosity of the molten metal and an enhancement of the molten pool turbulence, producing a uniform intermixture of elements having more uniform metal mixing during the welding process. In addition, the Si atoms in the Al–Si filler metal tend to diffuse in phase with the Cu atoms, which limits the local enrichment of Cu elements and the formation of IMCs [38]. In Al–Cu laser butt welding, the Al–Cu joint without filler metals can cause plastic deformation or even cracking in the fusion zone due to the significant difference in the thermal expansion resulting in thermal stresses in the weld. To overcome this, Weigl et al. used Si-based filler metals (Al–Si and Cu–Si alloys) with good compatibility with Al and Cu to improve the ductility and mechanical strength of the weld [104]. The results show that  $\text{AlSi}_{12}$  can significantly reduce the concentration of molten Cu in the fusion zone near the Cu substrate to a level of approximately 50%, which reduces the formation of IMCs, thereby reducing the crack sensitivity and increasing the joint toughness.

In summary, the different filler metals in Al and Cu laser welding can effectively suppress metal mixing and reduce the generation of brittle IMCs. At the same time, the melting point and thermal expansion coefficient of the filler metals are between the base material, which provides a strong boundary condition for balancing the different material properties of Al and Cu, reducing the thermal cracking and increasing the ductility of Al–Cu joints. However, the effects of different filler metals on the electrical properties of Al–Cu joints are rarely reported. The wettability of the filler metals to the base material needs to be taken into account, and the base material's surface must be polished or plated before laser welding. The metal atoms in the filler material may react

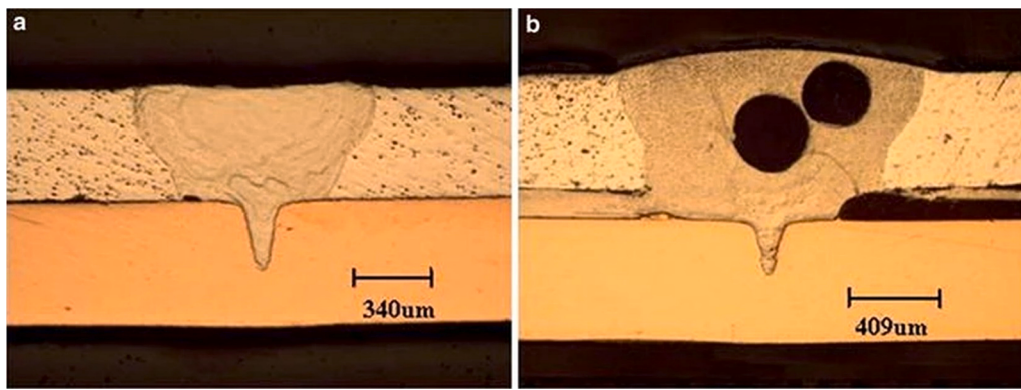


Fig. 21. Al-Cu laser welded with or without tin alloy [102]. (a) Without tin alloy. (b) With tin alloy.

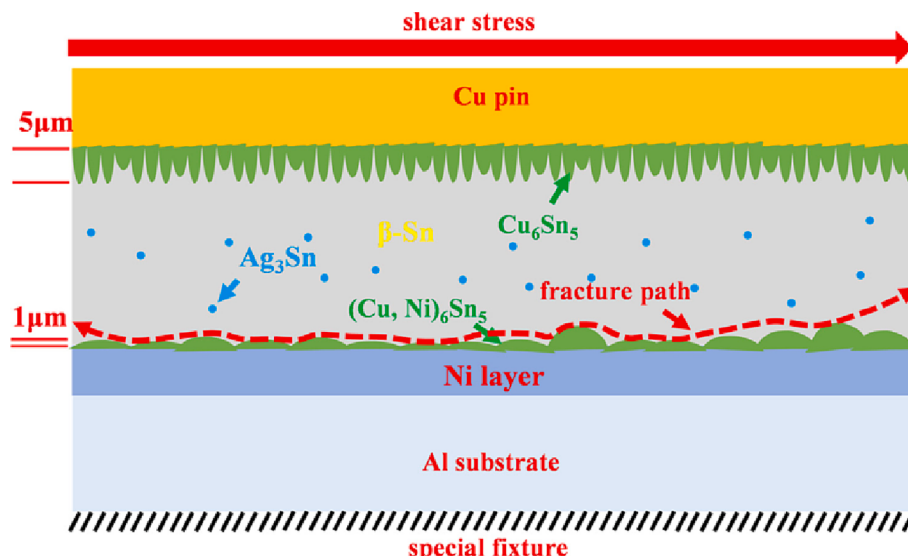


Fig. 22. The schematic diagram of the tensile fracture mechanism of laser welded aluminum and copper joints using Sn-based filler metals [103].

with the base material to form a new brittle phase, which can also cause cracking in the joint if not controlled. Therefore, it is necessary to select appropriate laser welding parameters according to the different filler metals to improve the mechanical properties of Al-Cu joints significantly.

## 5. Process monitoring

Laser welding is a typical multi-physical process coupling of light, electricity, magnetism, and heat. The metal melts by absorption of heat from the laser radiation to form a molten pool (heat conduction

**Table 5**  
Different monitoring techniques in laser welding.

Techniques	characterization	Monitored object	Advantages	Disadvantages	Refs
Spectrometer	Metal elements	• Plume	• Low cost • Small size	• Low sampling rate • Not intuitive	[108–111]
High-speed camera	Morphology	• Molten pool • Keyhole	• Intuitive • High sampling rate	• High cost • Susceptible to interference	[59,112–117]
Pyrometer	Temperature	• Molten pool • HAZ	• Low cost • Small size • High sampling rate	• Limited to local temperature • Not intuitive	[118,119]
Infrared camera	Temperature distribution	• Molten pool • HAZ	• Intuitive	• Difficulty in calibration • High cost	[120–122]
X-ray	Morphology	• Keyhole Porosity	• Intuitive • Detection of internal defects	• Low sampling rate • Radiation risk • High cost	[68,123–126]
Photodiode	Light intensity	• Molten pool • Plume	• Low cost • High sampling rate • Small size	• Not intuitive • Susceptible to interference	[116,121,127–130]
OCT	Penetration depth	• Keyhole	• Intuitive • High sampling rate • High accuracy	• High cost • Susceptible to interference • Difficult installation	[45,59,130–134]

welding). As the heat input increases, the recoil pressure from the molten pool due to evaporation causes the surface of the molten pool to drop and finally form a keyhole (keyhole-induced welding) [41,105]. The evaporated atoms and atomic clusters lead to the formation of ultrafine particles of fumes on the metal surface that are ejected upwards from the entrance of the keyhole to form a plume [106]. In contrast, the melt around the keyhole wall or entrance is sometimes ejected as spatter or molten droplets [61,107]. Different sensors are selected for laser welding process monitoring based on this physical process, displayed in Table 5. And the schematic diagram of process monitoring with various sensors during Al-Cu laser welding is shown in Fig. 23. The current process monitoring research on laser welding of Al and Cu is still only in the early exploration stage, mainly because the formation of Al-Cu IMCs occurs in the solidification phase after welding and process monitoring cannot directly and accurately obtain efficient information, needs to be analyzed with the aid of the microstructure of the welded cross-section. Thus, current research on process monitoring comes only from some indirect changes in characteristics (such as the degree of Al melting, penetration depth, etc.) to evaluate the joint quality.

### 5.1. Photodiode technique

The photodiode, shown in Fig. 23 (a), is coaxially mounted with the laser source to share the optical path. In laser welding, the beam splitter divides the light intensity radiated by the molten pool and plume into different wavelengths (visible, reflected, and infrared). The photodiode sensor converts the optical signals of different wavelengths into electrical signals collected by the acquisition card. The reflected laser can directly characterize the laser absorption of the base material. The higher the laser absorption, the lower the intensity of the reflected laser. The increase of the plume or the increase of the molten pool width can cause the intensity of the signals obtained through both infrared and visible. The same signal appears in different welding features, and it is impossible to determine which signal is the exact cause of the change.

Limited by the mutual solubility of Al and Cu, the amount of Al or Cu melted during the laser welding process determines the thickness of the IMC layer at the interface. As shown in Fig. 24, Mathivanan et al. utilized photodiodes to monitor the amount of Al melting during Cu and Al laser welding (Cu base material is on the top) [129]. The melting of Al is utilized as an indicator of the strength or weakness of the weld joint by recording the 396 nm Al peak captured by a photodiode with a specific Al bandpass filter during the welding process. As shown in Fig. 24 (a), there is a strong positive correlation between the voltage of the frequency component at 201 Hz and the laser power. Fig. 24 (b) shows a strong positive correlation between the voltage of the frequency component at 201 Hz and the shear force of the joint, with a correlation coefficient of 0.94. Lee et al. [135] classified the penetration depth of Al-Cu joints with the help of photodiodes and OCT sensors. A band-pass filter with 580 nm was used to collect the photodiode signals at the Cu emission wavelength as the training set. At the same time, the penetrate-on-depth signals collected by OCT were used as the test set, and the accuracy of the machine learning models (SVM, FCN, and CNN) was over 90%.

### 5.2. OCT technique

The OCT technique can capture 2D images with 1 μm resolution from objects with optical reflection and scattering properties. As shown in Fig. 23 (b), a beam of low coherent light is actively emitted from a welding head and split into a reference beam and a measurement beam by a beam splitter. The reflected beams from the reference plane and the sample surface or keyhole tip are synthesized separately. Both beams interfere, and the interfering beam is driven to the detector by the beam splitter and then dispersed by spectroscopy. The strong and weak spectral results of the electromagnetic waves are Fourier transformed. As the depth of the keyhole increases, the frequency increases, and the depth value of the sample surface or the keyhole tip is measured according to different frequencies. The difference between the two depths

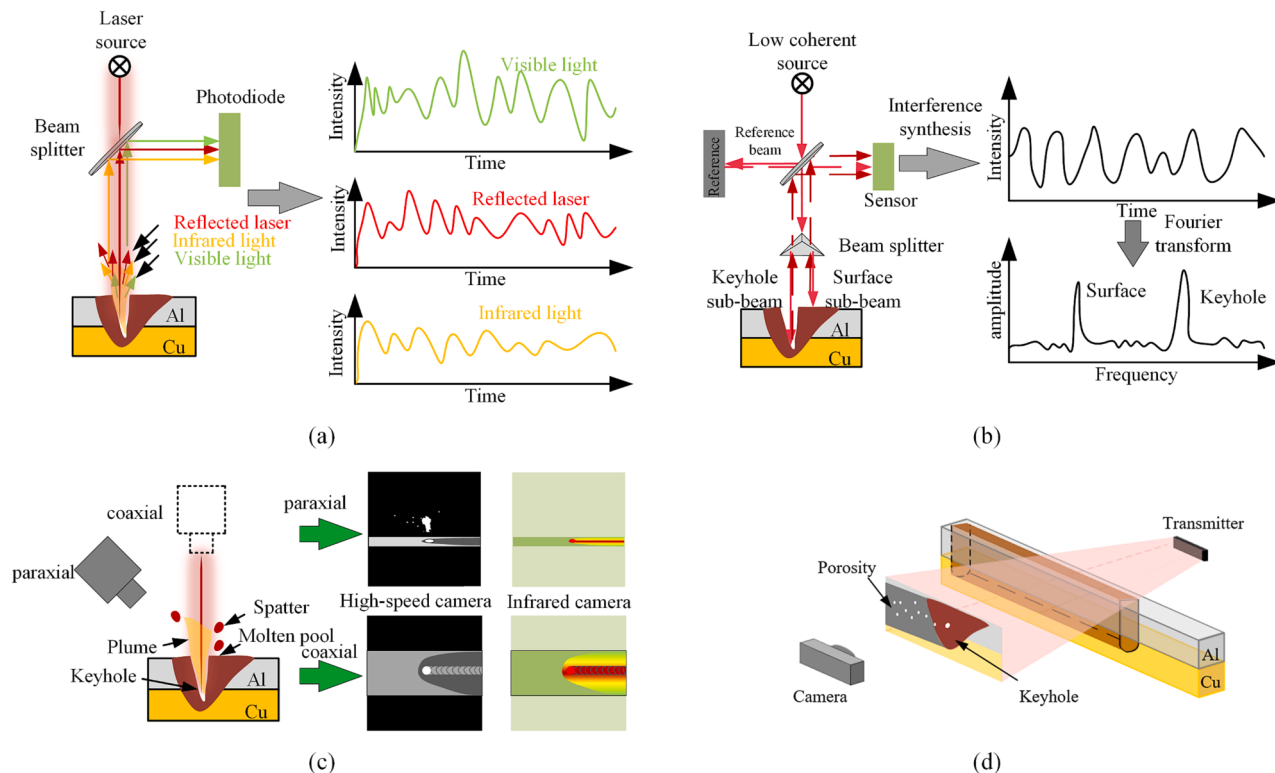


**Fig. 23.** The schematic diagram of the process monitoring process with different sensors during Al-Cu laser welding. (a) Photodiode. (b) OCT. (c) High-speed camera and Infrared camera. (d) X-ray.

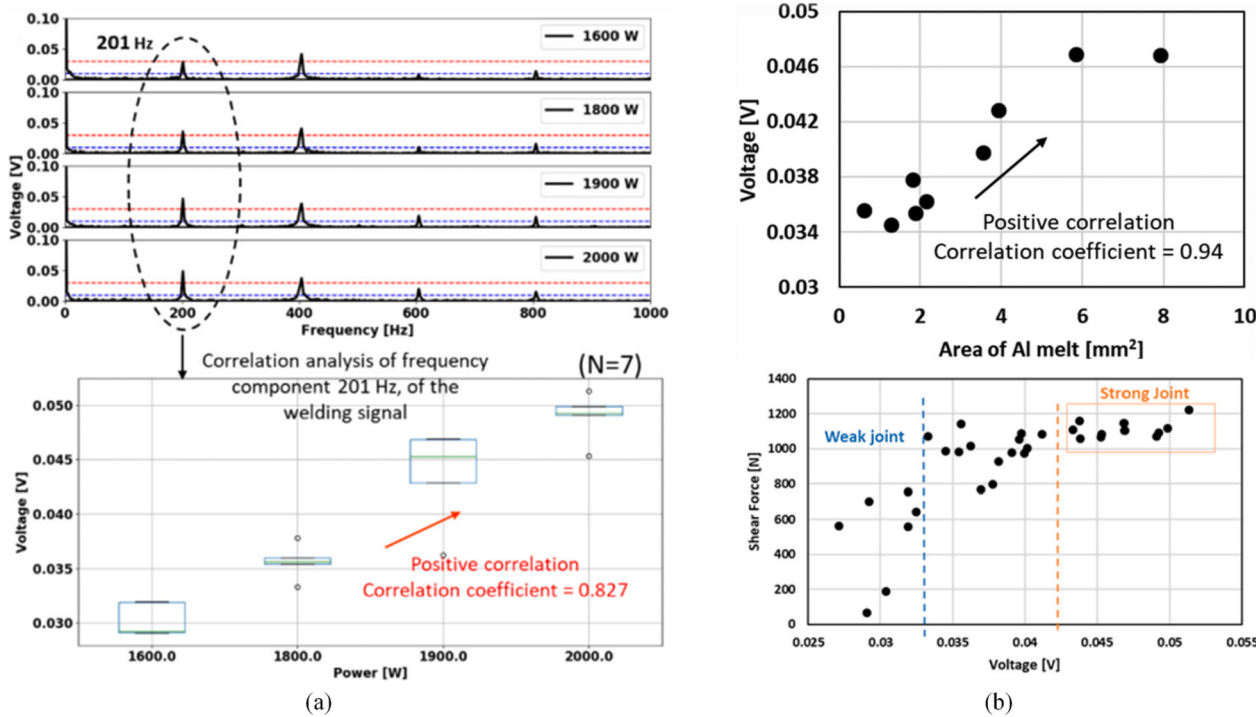


**Fig. 24.** Monitoring the laser welding process of Al and Cu by photodiodes [130]. (a) Frequency domain analysis of photodiode. (b) Correlation between the photodiode voltage at 201 Hz, the area of Al melt, and the shear force.

can represent the actual keyhole depth.

The penetration depth of Al and Cu welded joints for electrode ears of batteries is usually half penetration. An effective joint cannot form if the penetration depth is low, and penetration too deep presents a risk of piercing the battery [7]. Furthermore, deeper penetration depths can lead to more brittle IMCs due to intense diffusion reactions between Al and Cu, reducing the joint's mechanical and electrical properties. Therefore, sampling and manual preparation of weld cross sections are necessary to observe and measure the joint's penetration depth. To improve production efficiency, it is essential to implement online monitoring of the penetration depth in the Al and Cu laser welding process. The potential for this demand is provided by the OCT technique. As shown in Fig. 25, Sokolov et al. applied the OCT technique to monitor the laser welding process of Al and Cu, as well as using a high-speed camera to observe the dynamic behavior of the molten pool surface

and the keyhole during the laser welding process, by comparing the accuracy of OCT detection accuracy of penetration depth under the conditions of the single laser beam and dual-beam laser [45]. Fig. 25 (a) shows that the OCT sensor is mounted directly below the motorized collimator of the welding head so that it can share the optical path with the laser beam to monitor the keyhole depth. Fig. 25 (b) shows the raw data collected by the OCT sensor. A large amount of noise is introduced into the raw data, mainly due to the dynamic changes in keyhole size and shape during the welding process, and it is difficult to find and maintain the alignment between the OCT measurement beam and the bottom of the keyhole. The critical signal features are extracted using the keyhole mapping method for the raw data. A moving window is used to scan the entire signal, and the kernel density estimation is processed for the data points at each position in the moving window. The OCT technique provides a viable solution for online monitoring of weld

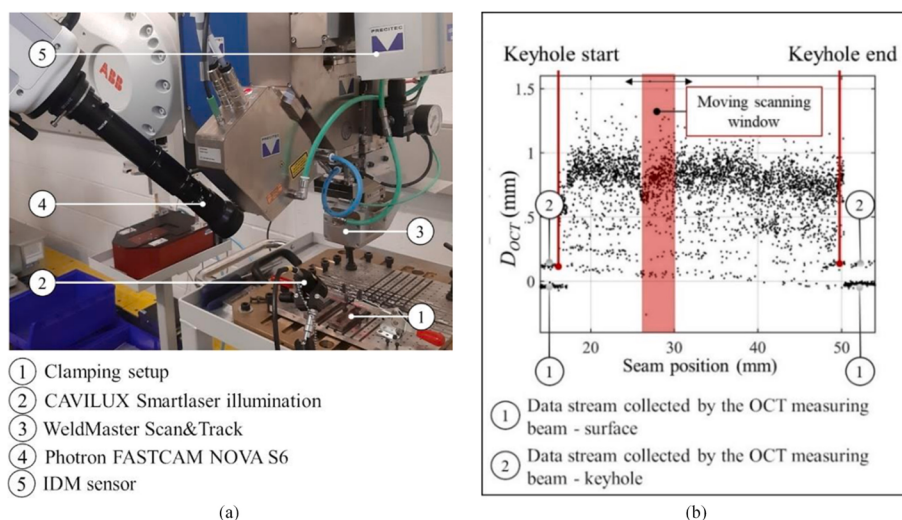


**Fig. 25.** Monitoring the laser welding process of Cu and Al using the OCT technique [45]. (a) Experimental setup. (b) Raw data of OCT signal.

penetration depth for Al and Cu laser welding. With improved sensor accuracy and optimizing the laser welding process, penetration depth detection technology can be applied in manufacturing, significantly improving the automation degree and production efficiency.

### 5.3. Visual sensing technique

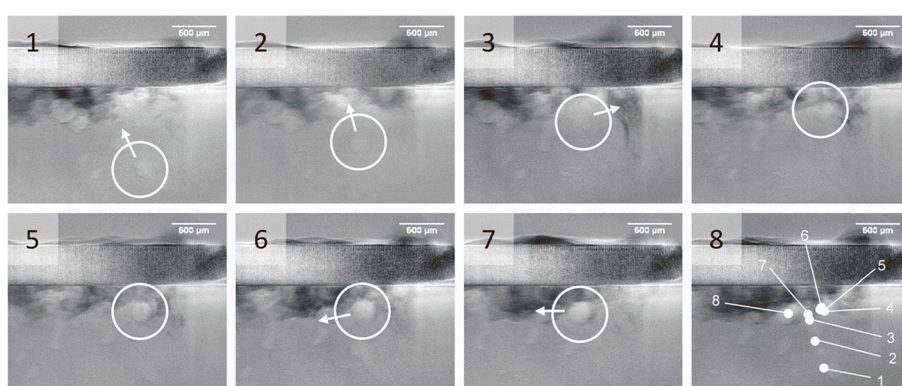
The visual sensing technique, shown in Fig. 23 (c) and (d), including visible, near-infrared ray, and X-ray, is more intuitive than the photo-diode sensor and OCT sensor, for it can be applied to higher spatial measurement and yield more information. The high-speed or infrared camera can be mounted coaxial or paraxial to detect morphology features such as molten pool and plume. The infrared camera additionally provides a time-dependent temperature distribution of the laser welding process. The X-ray with a high penetration ability is absorbed to different degrees in different internal structures of the weld. After imaging processing, the keyhole's internal features and the weld's porosity can be obtained. To study the metal mixing and porosity formation during Al-Cu laser welding, Hollatz et al. observed the mechanism of laser action with the help of an X-ray and high-speed camera [136]. As shown in Fig. 26, it was revealed that the instability of the keyhole was the main reason for the formation of porosity. Unfortunately, the higher optical density of Cu prevented visibility inside the copper. In addition, with the higher melting point of Cu and the higher energy content in the melt, the Al melt can overheat locally on the contact layer and promote the formation of porosity. As shown in Fig. 26 (a), the material transition and mixing prevented the porosity from escaping along the molten pool flow and being trapped in the transition zone. Fig. 26 (b) shows that the molten flow caused the Al-Cu mixing. The evaporation pressure

accelerated the upward flow of melt at the bottom of the keyhole, and the vortex effect on the molten pool surface accelerated the mixing degree, which was consistent with the simulation results of Huang et al. [73].

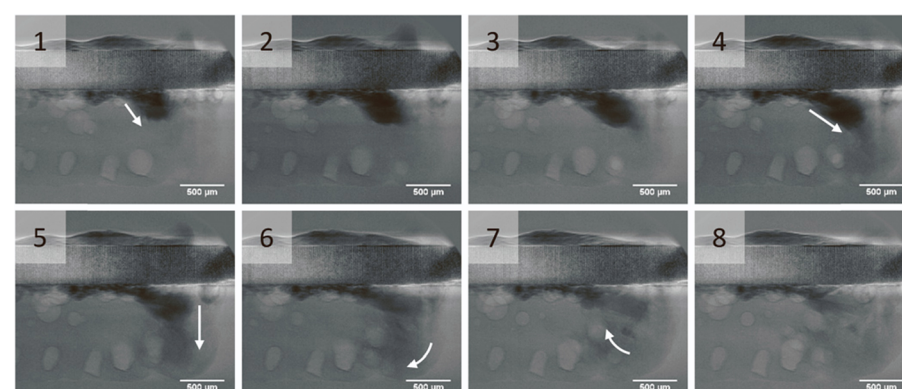
## 6. Summary and outlook

Laser welding of Al and Cu provides a critical way to connect the electrode ears in the battery system. Due to the different material properties, the low mutual solubility, and the poor fluidity of base materials, defects such as porosity, crack, and brittle IMCs inevitably occur at the welded joint. The optimization of the laser welding process relies on the appropriate control of parameters such as spot diameter, laser power, and welding speed to change the mixing ratio of base material and inhibit the formation of brittle IMCs in Al-Cu joints. Different laser output modes can improve the flow and temperature distribution of the molten pool, thus reducing the porosity and cracks and mixing Al and Cu. Filler metals with affinity to the base material can form a transition zone at the interface to avoid direct contact between Al and Cu and reduce the metal mixing. As a result, Al-Cu laser welded joints with good mechanical strength and electrical properties can be obtained by reducing the defects and IMC thickness. In addition, real-time welding process monitoring allows for evaluating the weld quality online. The melting amount of Al/Cu and the penetration depth reflect the degree of mixing of metal atoms, which determines the thickness of the IMC layer at the interface. Further development of Al-Cu laser welding technology will bring surprising results in emerging manufacturing.

More studies are expected to be carried out on laser welding of Al and Cu, as summarized below:



(a)



(b)

**Fig. 26.** The movement of porosity and molten Cu during the laser welding of Al and Cu was detected with the X-ray [137]. (a) The movement of porosity. (b) The movement of molten Cu.

- Further solutions are needed to precisely control the thickness of the IMC layer by optimizing the process parameters. To achieve close-loop control of Al and Cu laser welding, further investigations are needed to determine the optimal process parameters for various welding conditions. It is preferred to develop mathematical models between process parameters, heat input, and the thickness of the IMC layer.
- Blue or green lasers for welding Al and Cu are worth expecting. The successful application of high-power blue or green laser welding in non-ferrous metals offers the possibility to weld Al and Cu, and subsequent research can be centered on the effect of short wavelength lasers on the quality of Al-Cu joints.
- Finding new filler metals. Explore or create filler metals for laser welding of Al and Cu to improve the microstructure of the IMC and thus improve the joint quality.
- More sensing devices are needed for online monitoring of laser welding Al and Cu. Multi-sensor information fusion techniques, artificial intelligence, and deep learning algorithms should be applied to explore the relationship between welding process signals and weld joint quality.
- Numerical simulation and modeling of the microstructural evolution of Al-Cu laser welded joints should be investigated.
- Fatigue strength testing is considered necessary to evaluate joint quality. Al-Cu weld joints are inevitably subject to fatigue loss during packaging or service when used to connect the battery lugs.
- Charge or discharge testing of Al-Cu joint resistance needs further investigation. The battery lugs generate heat during charging and discharging resulting in energy loss, which has yet to be studied and standardized.

### Declaration of Competing Interest

The authors declare that they have no known competing financial interests or personal relationships that could have appeared to influence the work reported in this paper.

### Data availability

No data was used for the research described in the article.

### Acknowledgments

This work was supported in part by the Guangdong Provincial Natural Science Foundation of China under Grant 2023A1515012172, the National Natural Science Foundation of China under Grant 52275317, and the Guangzhou Municipal Special Fund Project for Scientific and Technological Innovation and Development (2023B03J1326).

### References

- [1] T. Solchenbach, P. Plapper, Combined laser beam braze-welding process for fluxless Al-Cu connections, in: Proceedings of the International Conference on competitive Manufacturing, COMA 13, 2013.
- [2] J.P. Bergmann, F. Petzoldt, R. Schurer, S. Schneider, Solid-state welding of aluminum to copper-case studies, *Weld. World* 57 (2013) 541–550.
- [3] R.K. Bhushan, D. Sharma, Green welding for various similar and dissimilar metals and alloys: present status and future possibilities, *Adv. Compos. Hybrid Mater.* 2 (2019) 389–406.
- [4] N.D. Alexopoulos, A.G. Anastasios, Z. Vasileios, V. Zanet, K. Nikolai, R. Stefan, K. Alexandra, Laser beam welded structures for a regional aircraft: weight, cost and carbon footprint savings, *J. Manuf. Syst.* 39 (2016) 38–52.
- [5] P. Zhu, D. Gastol, J. Marshall, R. Sommerville, V. Goodship, E. Kendrick, A review of current collectors for lithium-ion batteries, *J. Power Sources* 485 (2021), 229321.
- [6] H. Xia, L. Li, N. Ma, C. Tan, J. Gong, Influence of energy ratio on dual-spot laser welded-brazed Al/steel butt joint, *J. Mater. Process. Technol.* 281 (2020), 116624.
- [7] N. Kumar, I. Masters, A. Das, In-depth evaluation of laser-welded similar and dissimilar material tab-to-busbar electrical interconnects for electric vehicle battery pack, *J. Manufact. Process* 70 (2021) 78–96.
- [8] A. Sadeghian, N. Iqbal, A review on dissimilar laser welding of steel-copper, steel-aluminum, aluminum-copper, and steel-nickel for electric vehicle battery manufacturing, *Opt. Laser Technol.* 146 (2022), 107595.
- [9] S. Hollatz, S. Kremer, C. Ünlübayır, D.U. Sauer, A. Olowinsky, A. Gillner, Electrical modeling and investigation of laser beam welded joints for lithium-ion batteries, *Batteries* 6 (2020) 24.
- [10] I. Galvao, A. Loureiro, D.M. Rodrigues, Critical review on friction stir welding of aluminium to copper, *Sci. Technol. Weld. Join.* 21 (2016) 523–546.
- [11] O. Zobac, A. Kroupa, A. Zemanova, K.W. Richter, Experimental description of the Al-Cu binary phase diagram, *Metall. Mater. Trans. A* 50 (2019) 3805–3815.
- [12] M. Abbas, A.K. Taheri, M.T. Salehi, Growth rate of intermetallic compounds in Al/Cu bimetal produced by cold roll welding process, *J. Alloys Compd.* 319 (2001) 233–241.
- [13] W. Shin, D. Cho, D. Jung, H. Kang, J.O. Kim, Y. Kim, C. Park, Investigation on laser welding of Al ribbon to Cu sheet: weldability, microstructure, and mechanical and electrical properties, *Metals* 11 (2021) 831.
- [14] W. Shi, J. Huang, Y. Xie, Y. Li, F. An, Laser micro-welding technology for Cu-Al dissimilar metals and mechanisms of weld defect formation, *Int. J. Adv. Manuf. Technol.* 93 (2017) 4197–4201.
- [15] A. Imak, Overview of friction welding processes for different metallic materials, *Materials Testing* 64 (2022) 1372–1382.
- [16] J. Zhang, Y. Shen, X. Yao, H. Xu, B. Li, Investigation on dissimilar underwater friction stir lap welding of 6061-T6 aluminum alloy to pure copper, *Mater. Des.* 64 (2014) 74–80.
- [17] M. Mahmeen, S. Singh, Effect of tool pin offset on the mechanical properties of dissimilar materials based on Friction Stir Welding (FSW), *Int. J. Modern Trends Eng. Res.* (2016) 75–80.
- [18] A. Esmaili, M.K. Besharati Givi, H.R. Zaree Rajani, Experimental investigation of material flow and welding defects in friction stir welding of aluminum to brass, *Mater. Manufact. Process* 27 (2012) 1402–1408.
- [19] N. Sharma, Z.A. Khan, A.N. Siddiquee, Friction stir welding of aluminum to copper—an overview, *Trans. Nonferrous Metal Soc. China* 27 (2017) 2113–2136.
- [20] H. Shin, M. de Leon, Mechanical performance and electrical resistance of ultrasonic welded multiple Cu-Al layers, *J. Mater. Process. Technol.* 241 (2017) 141–153.
- [21] X. Wu, T. Liu, W. Cai, Microstructure, welding mechanism, and failure of Al/Cu ultrasonic welds, *J. Manufact. Process* 20 (2015) 321–331.
- [22] T. Itoi, A.B. Mohamad, R. Suzuki, K. Okagawa, Microstructure evolution of a dissimilar junction interface between an Al sheet and a Ni-coated Cu sheet joined by magnetic pulse welding, *Mater. Charact.* 118 (2016) 142–148.
- [23] A.K. Rajak, S.D. Kore, Numerical simulation and experimental study on electromagnetic crimping of aluminium terminal to copper wire strands, *Electr. Pow. Syst. Res.* 163 (2018) 744–753.
- [24] A. Garg, B. Panda, K. Shankhwar, Investigation of the joint length of weldment of environmental-friendly magnetic pulse welding process, *Int. J. Adv. Manuf. Technol.* 87 (2016) 2415–2426.
- [25] P. Kah, M. Martikainen, Trends in joining dissimilar metals by welding, *Appl. Mech. Mater.* 440 (2014) 269–276.
- [26] X. Wu, J. Du, W. Cai, Significance of workpiece conductivity on resistance spot welding process map, in: ASME 2019 14th International Manufacturing Science and Engineering Conference, 2019.
- [27] M. Zare, M. Pouranvari, Metallurgical joining of aluminium and copper using resistance spot welding: microstructure and mechanical properties, *Sci. Technol. Weld. Join.* 26 (2021) 461–469.
- [28] Y. Zhang, Y. Li, Z. Luo, T. Yuan, J. Bi, Z.M. Wang, Z.P. Wang, Y.J. Chao, Feasibility study of dissimilar joining of aluminum alloy 5052 to pure copper via thermo-compensated resistance spot welding, *Mater. Des.* 106 (2016) 235–246.
- [29] F.S. Li, R.Z. Xu, Z.C. Wei, X.F. Sun, P.F. Wang, X.F. Li, Z. Li, Investigation on the electron beam welding of Al/Cu composite plates, *Trans. Ind. Inst. Mater.* 73 (2020) 353–363.
- [30] X. Liu, Q. Dong, P. Wang, H. Chen, Review of electron beam welding technology in space environment, *Optik* 225 (2021), 165720.
- [31] B.E. Paton, L.M. Lobanov, Y.V. Naidich, New electron beam gun for welding in space, *Sci. Technol. Weld. Join.* 24 (2018) 320–326.
- [32] S. Yan, Y. Shi, Influence of laser power on microstructure and mechanical property of laser-welded Al/Cu dissimilar lap joints, *J. Manufact. Process* 45 (2019) 312–321.
- [33] S. Grabmann, J. Kriegler, F. Harst, F.J. Günter, M.F. Zaeh, Laser welding of current collector foil stacks in battery production—mechanical properties of joints welded with a green high-power disk laser, *Int. J. Adv. Manuf. Technol.* 118 (2022) 2571–2586.
- [34] V. Dimatteo, A. Ascarì, A. Fortunato, Continuous laser welding with spatial beam oscillation of dissimilar thin sheet materials (Al-Cu and Cu-Al): process optimization and characterization, *J. Manufact. Process* 44 (2019) 158–165.
- [35] R. Zhu, S. Guo, C. Huang, Z. Lei, X. Zhang, J. Liu, Effects of different types of interlayers on the interfacial reaction mechanism at the Cu side of Al/Cu lap joints obtained by laser welding/brazing, *Materials* 14 (2021) 7797.
- [36] X. Wang, F. Yan, X. Li, C. Wang, Induction diffusion brazing of copper to aluminium, *Sci. Technol. Weld. Join.* 22 (2017) 170–175.
- [37] T. Solchenbach, P. Plapper, W. Cai, Electrical performance of laser braze-welded aluminum-copper interconnects, *J. Manufact. Process* 16 (2014) 183–189.
- [38] Z. Lei, X. Zhang, J. Liu, P. Li, Interfacial microstructure and reaction mechanism with various weld fillers on laser welding-brazing of Al/Cu lap joint, *J. Manufact. Process* 67 (2021) 226–240.
- [39] P. Schmalen, P. Plapper, Evaluation of laser braze-welded dissimilar Al-Cu joints, *Phys. Procedia* 83 (2016) 506–514.

- [40] T. Solchenbach, P. Plapper, Mechanical characteristics of laser braze-welded aluminium-copper connections, *Opt. Laser Technol.* 54 (2013) 249–256.
- [41] D.Y. You, X.D. Gao, S. Katayama, Review of laser welding monitoring, *Sci. Technol. Weld. Join.* 19 (2014) 181–201.
- [42] B. Zhu, G. Zhang, J. Zou, N. Ha, Q. Wu, R. Xiao, Melt flow regularity and hump formation process during laser deep penetration welding, *Opt. Laser Technol.* 139 (2021), 106950.
- [43] Z. Zhang, S. Dong, Y. Wang, B. Xu, J. Fang, P. He, Microstructure characteristics of thick aluminum alloy plate joints welded by fiber laser, *Material & Design* 84 (2015) 173–177.
- [44] C. Chen, H. Zhou, C. Wang, L. Liu, Y. Zhang, K. Zhang, Laser welding of ultra-high strength steel with different oscillating modes, *J. Manufact. Process* 68 (2021) 761–769.
- [45] M. Sokolov, P. Franciosa, T. Sun, Applying optical coherence tomography for weld depth monitoring in remote laser welding of automotive battery tab connectors, *J. Laser Appl.* 1 (2021), 012028.
- [46] M. Kos, E. Arko, H. Kosler, M. Jezersek, Penetration-depth control in a remote laser-welding system based on an optical triangulation loop, *Opt. Lasers Eng.* 139 (2021), 106464.
- [47] J. Rinne, O. Seffer, S. Nothdurft, J. Hermsdorf, S. Kaierle, L. Overmeyer, Investigations on the weld metal composition and associated weld metal cracking in laser beam welded steel copper dissimilar joints, *J. Mater. Process. Technol.* 296 (2021), 117178.
- [48] S.F. Chua, H. Chen, G. Bi, Influence of pulse energy density in micro laser weld of crack sensitive Al alloy sheets, *J. Manufact. Process* 38 (2019) 1–8.
- [49] J. Enz, C. Carrarin, S. Riekehr, V. Ventzke, N. Kashaev, Hot cracking behaviour of an autogenously laser welded Al-Cu-Li alloy, *Int. J. Adv. Manuf. Technol.* 95 (2018) 299–310.
- [50] L. Wang, Y. Liu, C. Yang, M. Gao, Study of porosity suppression in oscillating laser-MIG hybrid welding of AA6082 aluminum alloy, *J. Mater. Process. Technol.* 292 (2021), 117053.
- [51] X. Cao, M. Jahazi, J.P. Immarigeon, W. Wallace, A review of laser welding techniques for magnesium alloys, *J. Mater. Process. Technol.* 171 (2006) 188–204.
- [52] R. Baumann, D. Hipp, A.F. Lasagni, A. Mahrle, Tailored absorptivity: Increasing the laser weldability of copper through surface structuring, *Mater. Lett.* 283 (2021), 128700.
- [53] T. Beck, C. Bantel, M. Boley, J.P. Bergmann, OCT capillary depth measurement in copper micro welding using green lasers, *Appl. Sci.* 11 (2021) 2655.
- [54] L. Chen, G. Mi, X. Zhang, C. Wang, Effects of sinusoidal oscillating laser beam on weld formation, melt flow and grain structure during aluminum alloys lap welding, *J. Mater. Process. Technol.* 298 (2021), 117314.
- [55] Z. Sun, J.C. Ion, Laser welding of dissimilar metal combinations, *J. Mater. Sci.* 30 (1995) 4205–4214.
- [56] M.F.R. Zwicker, M. Moghadama, W. Zhang, C.V. Nielsen, Automotive battery pack manufacturing – a review of battery to tab joining, *J. Adv. Join. Process.* 1 (2020), 100017.
- [57] H. Ehsan, K. Paul, Laser welding of aluminum battery tab to variable Al/Cu busbars in Li-ion battery joint, *AIMS Mater. Sci.* 9 (2022) 884–918.
- [58] S. Yan, Z. Li, L. Song, Y. Zhang, S. Wei, Research and development status of laser micro-welding of aluminum-copper dissimilar metals: a review, *Opt. Lasers Eng.* 161 (2023) 107312.
- [59] D. Ma, P. Jiang, L. Shu, S. Geng, Real-time porosity monitoring during laser welding of aluminum alloys based on keyhole 3D morphology characteristics, *J. Manuf. Syst.* 65 (2022) 70–87.
- [60] C.D. Boley, S.A. Khairallah, A.M. Rubenchik, Calculation of laser absorption by metal powders in additive manufacturing, *Appl. Opt.* 54 (2015) 2477–2482.
- [61] S. Katayama, Fundamentals and Details of Laser Welding, Springer, 2020.
- [62] S.W. Britten, L. Schmid, T. Molitor, M. Rütering, Blue high-power laser sources for processing solutions in e-mobility and beyond, *Procedia CIRP* 94 (2020) 592–595.
- [63] P. Stritt, C. Hagenlocher, C. Kizler, R. Weber, C. Rüttimann, T. Graf, Laser spot welding of copper-aluminum joints using a pulsed dual wavelength laser at 532 and 1064 nm, *Phys. Procedia* 56 (2014) 759–767.
- [64] I.Z. Awan, A.Q. Khan, Precipitation from solid solutions, *J. Chem. Soc. Pakistan* 39 (2017) 319–336.
- [65] D. Zuo, S. Hu, J. Shen, Z. Xue, Intermediate layer characterization and fracture behavior of laser-welded copper/aluminum metal joints, *Mater. Des.* 58 (2014) 357–362.
- [66] M. Braunovic, Reliability of power connections, *J. Zhejiang Univ.* 8 (3) (2007) 343–356.
- [67] T. Solchenbach, P. Plapper, M. Greger, J.L. Biagi, J. Bour, J.A.S. Bomfirm, Thermal and electrical aging of laser braze-welded aluminum-copper interconnects, *Transl. Mater. Res.* 1 (2014), 015001.
- [68] P. Schmalen, P. Plapper, I. Peral, I. Titov, O. Vallcorba, J. Rius, Composition and phases in laser welded Al-Cu joints by synchrotron x-ray microdiffraction, *Procedia CIRP* 74 (2018) 27–32.
- [69] S. Tavassoli, M. Abbasi, R. Tahavvori, Controlling of IMCs layers formation sequence, bond strength and electrical resistance in Al-Cu bimetal compound casting process, *Mater. Des.* 108 (2016) 343–353.
- [70] P. Schmalen, P. Plapper, Resistance measurement of laser welded dissimilar Al/Cu joints, *J. Laser Micro Nanoeng.* 12 (2017) 189–194.
- [71] Z.Q. Xue, S.S. Hu, J.Q. Shen, D. Zuo, E. Kannatey-Asibu, Microstructure characterization and mechanical properties of laser-welded copper and aluminum lap joint, *J. Laser Appl.* 26 (2014), 012002.
- [72] S.J. Lee, H. Nakamura, Y. Kawahito, S. Katayama, Effect of welding speed on microstructural and mechanical properties of laser lap weld joints in dissimilar Al and Cu sheets, *Sci. Technol. Weld. Join.* 19 (2014) 111–118.
- [73] W. Huang, H. Wang, T. Rinker, W. Tan, Investigation of metal mixing in laser keyhole welding of dissimilar metals, *Mater. Des.* 195 (2020), 109056.
- [74] V. Dimatteo, A. Ascoli, E. Liverani, A. Fortunato, Experimental investigation on the effect of spot diameter on continuous-wave laser welding of copper and aluminum thin sheets for battery manufacturing, *Opt. Laser Technol.* 145 (2022), 107495.
- [75] Z. Xue, S. Hu, D. Zuo, W. Cai, D. Lee, K. Elijah, Molten pool characterization of laser lap welded copper and aluminum, *J. Phys. D, Appl. Phys.* 46 (2013), 495501.
- [76] Q. Cheng, P. Zhang, H. Shi, Z. Yu, Study on microstructure and mechanical properties of aluminum-copper dissimilar metals joints by nanosecond laser spiral welding, *Trans. Indian Inst. Met.* 75 (2022) 2517–2528.
- [77] Y. Feng, X. Gao, Y. Zhang, C. Peng, X. Gui, Y. Sun, X. Xiao, Simulation and experiment for dynamics of laser welding keyhole and molten pool at different penetration status, *Int. J. Adv. Manuf. Technol.* 112 (2021) 2301–12132.
- [78] F. Hugger, K. Hofmann, S. Kohl, M. Dobler, M. Schmidt, Spatter formation in laser beam welding using laser beam oscillation, *Weld. World* 59 (2015) 165–172.
- [79] F. Fetzer, M. Sommer, R. Weber, J. Webergals, T. Graf, Reduction of pores by means of laser beam oscillation during remote welding of AlMgSi, *Opt. Lasers Eng.* 108 (2018) 68–77.
- [80] S. Kou, Welding Metallurgy, 2nd ed., John Wiley & Sons, Hoboken, 2003.
- [81] D.J.D.F.W. Kurz, Fundamentals of Solidification (1986).
- [82] Z. Yuan, Y. Tu, T. Yuan, Y. Zhang, Y. Huang, Size effects on mechanical properties of pure industrial aluminum sheet for micro/meso scale plastic deformation: experiment and modeling, *J. Alloy. Compd.* 859 (2021) 157752.
- [83] K. Mathivanana, P. Plapper, Laser overlap joining from copper to aluminum and analysis of failure zone, *Lasers Manufact. Conf.* 208077248 (2019).
- [84] F. Fetzer, M. Jarwitz, P. Stritt, R. Weber, T. Graf, Fine-tuned remote laser welding of aluminum to copper with local beam oscillation, *Phys. Procedia* 83 (2016) 455–462.
- [85] V. Dimatteo, A. Ascoli, A. Fortunato, Dissimilar laser welding of copper and aluminum alloys in multilayer configuration for battery applications, *J. Laser Appl.* 33 (2021), 042028.
- [86] E. Assuncao, S. Williams, Comparison of continuous wave and pulsed wave laser welding effects, *Opt. Lasers Eng.* 51 (2013) 674–680.
- [87] K. Mathivanan, P. Plapper, Laser welding of dissimilar copper and aluminum sheets by shaping the laser pulses, *Procedia Manuf.* 36 (2019) 154–162.
- [88] F. Lerra, A. Ascoli, A. Fortunato, The influence of laser pulse shape and separation distance on dissimilar welding of Al and Cu films, *J. Manufact. Process* 45 (2019) 331–339.
- [89] B. Zhu, L. Zhen, H. Xia, J. Su, S. Niu, L. Wu, C. Tan, B. Chen, Effect of the scanning path on the nanosecond pulse laser welded Al/Cu lapped joint, *Opt. Laser Technol.* 139 (2021), 106945.
- [90] Q. Li, B. Zhu, H. Li, S. Niu, L. Wu, Z. Zeng, H. Xia, B. Chen, C. Tan, Effect of spiral scan distance on the nanosecond-pulsed-laser lap joint of Al/Cu, *Opt. Laser Technol.* 158 (2023), 108896.
- [91] A. Ascaria, A. Fortunato, E. Liverania, A. Lutey, Application of different pulsed laser sources to dissimilar welding of Cu and Al alloys, *Lasers Manufact. Conf.* (2019).
- [92] N.T. Tien, Y.L. Lo, M.M. Raza, C. Chen, C. Chiu, Optimization of processing parameters for pulsed laser welding of dissimilar metal interconnects, *Opt. Laser Technol.* 159 (2023), 109022.
- [93] L. Wang, X. Gao, F.R. Kong, Keyhole dynamic status and spatter behavior during welding of stainless steel with adjustable-ring mode laser beam, *J. Manufact. Process* 74 (2022) 201–219.
- [94] M. Mohammadpour, L. Wang, F. Kong, R. Kovacevic, Adjustable ring mode and single beam fiber lasers: a performance comparison, *Manufact. Lett.* 25 (2021) 50–55.
- [95] L. Wang, M. Mohammadpour, B. Yang, X. Gao, J. Lavoie, K. Kleine, F. Kong, R. Kovacevic, Monitoring of keyhole entrance and molten pool with quality analysis during adjustable ring mode laser welding, *Appl. Opt.* 59 (2020) 1576–1584.
- [96] J.H. Cha, H.W. Choi, Characterization of dissimilar aluminum-copper material joining by controlled dual laser beam, *Int. J. Adv. Manuf. Technol.* 119 (2022) 1909–1920.
- [97] L. Zhou, Z.Y. Li, X.G. Song, C.W. Tan, Z.Z. He, Y.X. Huang, J.C. Feng, Influence of laser offset on laser welding-brazing of Al/brass dissimilar alloys, *J. Alloy. Compd.* 717 (2017) 78–92.
- [98] I. Mys, M. Schmidt, Laser micro welding of copper and aluminum, *Proc. SPIE* 6107 (2006) 28–33.
- [99] G. Eßer, I. Mys, M.H. Schmidt, Laser micro welding of copper and aluminium using filler materials, in: Fifth International Symposium on Laser Precision Microfabrication, 5662, SPIE, 2004, pp. 337–342.
- [100] H.S. Furuya, Y.S. Sato, H. Kokawa, T. Huang, R.S. Xiao, Improvement of interfacial strength with the addition of Ni in Al/Cu dissimilar joints produced via laser brazing, *Metall. Mater. Trans. A* 49 (2018) 6215–6223.
- [101] S. Yan, Y. Shi, Influence of Ni interlayer on microstructure and mechanical properties of laser welded joint of Al/Cu bimetal, *J. Manufact. Process* 59 (2020) 343–354.
- [102] M.M. Hailat, A. Mian, Z.A. Chaudhury, N. Golam, P. Rahul, H.J. Herfurth, Laser micro-welding of aluminum and copper with and without tin foil alloy, *Microsyst. Technol.* 18 (2012) 103–112.

- [103] P. Huan, X. Tang, Q. Sun, K. Akirab, X. Wang, J. Wang, X. Wei, H. Di, Comparative study of solder wettability on aluminum substrate and microstructure-properties of Cu-based component/aluminum laser soldering joint, *Mater. Des.* 215 (2022), 110485.
- [104] M. Weigla, F. Alberta, M. Schmidt, Enhancing the ductility of laser-welded copper-aluminum connections by using adapted filler materials, *Phys. Procedia* 12 (2011) 332–338.
- [105] X. Fan, X. Gao, G. Liu, N. Ma, Y. Zhang, Research and prospect of welding monitoring technology based on machine vision, *Int. J. Adv. Manuf. Technol.* 115 (2021) 3365–3391.
- [106] T. Wang, X. Gao, K. Seiji, X. Jin, Study of dynamic features of surface plasma in high-power disk laser welding, *Plasma Sci. Technol.* 14 (3) (2012) 245–251.
- [107] X. Gao, Y. Sun, S. Katayama, Neural network of plume and spatter for monitoring high-power disk laser welding, *Int. J. Precision Eng. Manufact.-Green Technol.* 1 (4) (2014) 293–298.
- [108] B. Zhang, L. Sun, H. Yu, Y. Xin, Z. Cong, A method for improving wavelet threshold denoising in laser-induced breakdown spectroscopy, *Spectrochim. Acta B At. Spectrosc.* 107 (2015) 32–44.
- [109] Z. Zhang, Y. Huang, R. Qin, Z. Lei, G. Wen, Real-time measurement of seam strength using optical spectroscopy for Al-Li alloy in laser beam welding, *IEEE Trans. Instrum. Meas.* 70 (2021) 1–10.
- [110] T. Sibilano, A. Ancona, V. Berardi, E. Schingaro, P. Parente, P.M. Lugarà, Correlation spectroscopy as a tool for detecting losses of ligand elements in laser welding of aluminium alloys, *Opt. Lasers Eng.* 44 (12) (2006) 1324–1335.
- [111] X. Gao, Y. Zhang, Monitoring of welding status by molten pool morphology during high-power disk laser welding, *Optik – Int. J. Light Electron Opt.* 126 (19) (2015) 1797–1802.
- [112] D. You, X. Gao, S. Katayama, Visual-based spatter detection during high-power disk laser welding, *Opt. Lasers Eng.* 54 (2014) 1–7.
- [113] X. Gao, Y. Sun, D. You, Z. Xiao, X. Chen, Multi-sensor Information fusion for monitoring disk laser welding, *Int. J. Adv. Manuf. Technol.* 85 (2016) 1167–1175.
- [114] X. Gao, L. Mo, D. You, Z. Li, Tight butt joint weld detection based on optical flow and particle filtering of magneto-optical imaging, *Mech. Syst. Sig. Process.* 96 (2017) 16–30.
- [115] B. Zhang, S. Liu, Y.C. Shin, In-Process monitoring of porosity during laser additive manufacturing process, *Addit. Manuf.* 28 (2019) 497–505.
- [116] D. You, X. Gao, S. Katayama, Detection of imperfection formation in disk laser welding using multiple on-line measurements, *J. Mater. Process. Technol.* 219 (2015) 209–220.
- [117] Y.X. Zhang, S.W. Han, J. Cheon, S.J. Na, X.D. Gao, Effect of joint gap on bead formation in laser butt welding of stainless steel, *J. Mater. Process. Technol.* 249 (2017) 274–284.
- [118] X. Xiao, X. Liu, M. Cheng, L. Song, Towards monitoring laser welding process via a coaxial pyrometer, *J. Mater. Process. Technol.* 277 (2020), 116409.
- [119] A.G. Demir, C. De Giorgi, B. Previtali, Design and implementation of a multisensor coaxial monitoring system with correction strategies for selective laser melting of a maraging steel, *J. Manuf. Sci. Eng.* 140 (2018), 041003.
- [120] Z. Chen, X. Gao, Detection of weld pool width using infrared imaging during high-power fiber laser welding of type 304 austenitic stainless steel, *Int. J. Adv. Manuf. Technol.* 74 (2014) 1247–1254.
- [121] L. Cheng, G. Mi, S. Li, C. Wang, X. Hu, Defects diagnosis in laser brazing using near-infrared signals based on empirical mode decomposition, *Opt. Laser Technol.* 100 (2018) 12–20.
- [122] M. Roberts, K. Wang, E. Guzas, W. Tucker, P. Lockhart, Induction infrared thermography for non-destructive evaluation of welding-induced sensitization in stainless steels, *J. Nondestr. Eval.* 40 (1) (2021).
- [123] M. Hummel, M. Kulkens, C. Schöler, W. Schulz, A. Gillner, In situ X-ray tomography investigations on laser welding of copper with 5115 and 1030 nm laser beam sources, *J. Manufact. Process* 67 (2021) 170–176.
- [124] Y. Sato, N. Shinohara, T. Arita, In situ x-ray observation of keyhole dynamics for laser beam welding of stainless steel with 16 kW disk laser, *J. Laser Appl.* 33 (2021), 042043.
- [125] H. Legall, J. Bonse, J. Krüger, Review of x-ray exposure and safety issues arising from ultra-short pulse laser material processing, *J. Radiol. Prot.* 41 (1) (2021) R28–R42.
- [126] X. Dong, C.J. Taylor, T.F. Cootes, A random forest-based automatic inspection system for aerospace welds in X-ray images, *IEEE Trans. Autom. Sci. Eng.* 18 (2021) 2128–2141.
- [127] D. You, X. Gao, S. Katayama, A novel stability quantification for disk Laser welding by using frequency correlation coefficient between multiple-optics signals, *IEEE/ASME Trans. Mechatron.* 20 (2015) 327–337.
- [128] D. You, X. Gao, S. Katayama, Multiple-optics sensing of high-brightness disk laser welding process, *NDT&E INT* 60 (2013) 32–39.
- [129] K. Mathivanan, P. Plapper, Correlation of optical signal during laser fusion welding of copper to aluminum, *J. Laser Appl.* 33 (2021), 012037.
- [130] Y. Zhang, D. You, X. Gao, N. Zhang, P.P. Gao, Welding defects detection based on deep learning with multiple optical sensors during disk laser welding of thick plates, *J. Manufact. Syst.* 51 (2019) 87–94.
- [131] J.J. Blecher, C.M. Galbraith, C. Van Vlack, T.A. Palmer, J.M. Fraser, P.J. L. Webster, T. DebRoy, Real time monitoring of laser beam welding keyhole depth by laser interferometry, *Sci. Technol. Weld. Join.* 19 (2014) 560–564.
- [132] M. Boley, F. Fetzer, R. Weber, T. Graf, Statistical evaluation method to determine the laser welding depth by optical coherence tomography, *Opt. Lasers Eng.* 119 (2019) 56–64.
- [133] R. Lahdo, O. Seffer, S. Kaierle, L. Overmeyer, Investigations on in-process control of penetration depth for high-power laser welding of thick steel-aluminum joints, *J. Laser Appl.* 31 (2019), 022418.
- [134] D. Holder, S. Boley, M. Buser, R. Weber, T. Graf, In-process determination of fiber orientation for layer accurate laser ablation of CFRP, *Procedia CIRP* 74 (2018) 557–561.
- [135] K. Lee, S. Kang, M. Kang, S. Yi, Estimation of Al/Cu laser weld penetration in photodiode signals using deep neural network classification, *J. Laser Appl.* 33 (2021), 042009.
- [136] S. Hollatz, M. Hummel, A. Olowinsky, A. Gillner, F. Beckmann, J. Moosmann, Pore formation and melt pool analysis of laser welded Al-Cu joints using synchrotron radiation, *J. Mater. Process. Technol.* 39 (2022), 117738.